

# One-point fluctuation analysis of the high-energy neutrino sky

Michael R. Feyereisen,<sup>a</sup> Irene Tamborra<sup>b,a</sup> and Shin'ichiro Ando<sup>a</sup>

<sup>a</sup>GRAPPA Institute, University of Amsterdam, Science Park 904, 1098 XH Amsterdam, Netherlands

<sup>b</sup>Niels Bohr International Academy, Niels Bohr Institute, Blegdamsvej 17, 2100 Copenhagen, Denmark

E-mail: [m.r.feyereisen@uva.nl](mailto:m.r.feyereisen@uva.nl), [tamborra@nbi.ku.dk](mailto:tamborra@nbi.ku.dk), [s.ando@uva.nl](mailto:s.ando@uva.nl)

**Abstract.** We perform the first one-point fluctuation analysis of the high-energy neutrino sky. This method reveals itself to be especially suited to contemporary neutrino data, as it allows to study the properties of the astrophysical components of the high-energy flux detected by the IceCube telescope, even with low statistics and in the absence of point source detection. Besides the veto-passing atmospheric foregrounds, we adopt a simple modeling of the high-energy neutrino background by assuming two main extra-galactic components: star-forming galaxies and blazars. By leveraging multi-wavelength data from *Herschel* and *Fermi*, we predict the spectral and anisotropic probability distributions for their expected neutrino counts in IceCube. We find that star-forming galaxies are likely to remain a diffuse background due to poor angular resolution, and determine an upper limit on the number of shower events that can reasonably be associated to blazars. We also find that upper limits on the contribution of blazars to the measured flux are unfavourably affected by the skewness of their flux distribution. Our modeling suggests that blazars and star-forming galaxies can jointly explain only  $\sim 5$  events of the 53 observed in the IceCube HESE data, leaving room for other astrophysical components at greater than  $5\sigma$  significance in a one-point fluctuation analysis.

**Keywords:** Neutrino astronomy, ultra high-energy photons and neutrinos, gamma-ray theory, particle acceleration.

---

## Contents

<b>1</b>	<b>Introduction</b>	<b>1</b>
<b>2</b>	<b>Neutrino flux distributions of single sources</b>	<b>2</b>
2.1	Correlating gamma-ray and neutrino fluxes	2
2.2	Star-forming galaxy fluxes from the <i>Herschel</i> data	3
2.3	Blazar fluxes from the <i>Fermi</i> 2FHL catalogue	4
2.4	Single source distribution	4
<b>3</b>	<b>Atmospheric foregrounds</b>	<b>6</b>
<b>4</b>	<b>Flux and count distributions of single pixels</b>	<b>6</b>
4.1	Obtaining the total (multi-source) flux distribution	7
4.2	Obtaining the observed count distribution	8
4.3	Distributions of the extragalactic source populations	9
<b>5</b>	<b>Results</b>	<b>12</b>
5.1	Resolvability of point sources	12
5.2	Detectability of star-forming galaxies and blazars as point sources	14
5.3	A “pointless” clustering analysis	16
5.4	One-point fluctuation analysis	19
<b>6</b>	<b>Discussion</b>	<b>21</b>
<b>7</b>	<b>Conclusions</b>	<b>22</b>
<b>A</b>	<b>Modeling of the IceCube effective area</b>	<b>23</b>
A.1	Convulsive integration and neutrino fluxes	24
A.2	Declination dependence	26
A.3	Flavour dependence	26
<b>B</b>	<b>Illustration of the bias on the blazar contribution</b>	<b>26</b>
<b>C</b>	<b>Methodological contrast to one-point <i>fitting</i></b>	<b>27</b>
<b>D</b>	<b>One-point fluctuation analysis: cross checks</b>	<b>28</b>

---

## 1 Introduction

In 2013, the IceCube Collaboration reported an excess of high-energy neutrinos over the atmospheric neutrino background [1–4]. The spatial distribution of these events, consistent with isotropy and with no significant clustering, may suggest an extragalactic origin of the detected neutrinos [5, 6]. Besides a Galactic contribution [7, 8], various extragalactic astrophysical sources have been suggested as factories of the IceCube neutrinos, e.g. star-forming galaxies (SFG) [9–14], active-galactic nuclei [15–20], galaxy clusters [21, 22], sources dim or scarcely visible in photons [23–29] as well as more exotic dark matter decays [30–33]. Recent

work employing accurate statistical analysis as well as up-to-date gamma-ray data-sets places stronger constraints on some of the proposed sources [34–36]. In this study we are interested in the joint contribution of all these source populations to the extragalactic neutrino flux.

Given the paucity of the high-energy neutrino data, it is important to extract as much information as we can from them. We here aim at exploiting the full probability distribution of the currently available neutrino data-set by employing a one-point fluctuation analysis. We first model the high-energy neutrino sky in a data-driven way, by assuming that neutrinos from SFGs and from blazars constitute the main bulk of the observed IceCube flux, other than the atmospheric background. The IceCube neutrino data are then connected to our phenomenological model by means of a one-point fluctuation analysis [37–41]. Our study suggests that SFGs and blazars (along with the atmospheric foregrounds) are insufficient to explain the data (with a one-sided  $p < 3 \times 10^{-7}$  post-trials), and that the missing un-modelled component is likely of astrophysical origin, with a spectral contribution both relevant between 25–100 TeV and extending above 100 TeV.

In addition to one-point fluctuation analyses, the probability distribution of the individual neutrino counts allows us to make detection forecasts of these astrophysical populations as point sources above diffuse backgrounds that they themselves generate. This extreme-value analysis suggests that a detector with the IceCube angular resolution would not be likely to detect SFGs as point sources above the background of other SFGs. On the other hand, blazars are sufficiently rare sources that they will not constitute a background to themselves; instead, the skewness of the blazar flux distribution biases results derived from population averages by a non-negligible factor compared to the full distributional result, which we compute.

The layout of the paper is as follows. In Sec. 2, we present our data-driven modelling of the extragalactic neutrino flux. Sec. 3 discusses the atmospheric foregrounds that we assume in our analysis. In Sec. 4, we present what we should observe on Earth as a consequence of the adopted astrophysical models and characterise the flux distributions of star-forming galaxies and blazars, arguing that they are sufficiently skewed to bias results on unresolved source contributions to the diffuse backgrounds. In Sec. 5, we discuss applications of the one-point fluctuation analysis as well as the main results of our analyses. The caveats of this study are presented in Sec. 6, and our findings are summarised in Sec. 7. Further materials complementing the methodological discussions are also reported in the Appendices.

## 2 Neutrino flux distributions of single sources

In this Section, after introducing a simple phenomenological relation between the neutrino and the gamma-ray fluxes, we describe the inputs we used to model the neutrino emission from SFGs and blazars and introduce the single-source distribution function.

### 2.1 Correlating gamma-ray and neutrino fluxes

In a proton-rich astrophysical environment, the neutrino emission can be directly correlated to the gamma-ray emission [5, 42]:

$$\frac{1}{3} \sum_{\alpha=1}^6 E_{\nu} Q_{\nu,\alpha} = \frac{\kappa}{2} E_{\gamma} Q_{\gamma} , \quad (2.1)$$

where  $\alpha$  runs over (anti)neutrino flavours,  $Q$  is the energy-differential emission rate per source (in units of  $\text{s}^{-1} \text{ GeV}^{-1}$ ) and  $\kappa$  is 2 for  $pp$ , or  $\leq 2$  for  $p\gamma$  interactions. Using the direct relation

between the neutrino and the gamma-ray energies ( $2E_\nu = E_\gamma$ ) and integrating over source densities on both sides of Eq. (2.1) to get the differential fluxes (in units of  $\text{cm}^{-2} \text{s}^{-1} \text{GeV}^{-1}$ ), we have  $(1/6) \sum_\alpha F_{\nu,\alpha} = (\kappa/2) F_\gamma$ . Since neutrino oscillations push the flavour ratio towards 1:1:1 for extragalactic sources, we can define the all-flavour neutrino and antineutrino flux as

$$F_\nu \equiv \sum_{\alpha=1}^6 F_{\nu,\alpha} = 3\kappa F_\gamma. \quad (2.2)$$

In this study, we will be considering the statistics of the flux in individual pixels, i.e. with (differential) intensities  $I = F/\Omega_{\text{pix}}$  (in units of  $\text{cm}^{-2} \text{s}^{-1} \text{sr}^{-1} \text{GeV}^{-1}$ ). In addition to these energy-differential quantities, gamma-ray studies often work with fluxes  $S$  (in units of  $\text{cm}^{-2} \text{s}^{-1}$ ) integrated over a certain energy range  $[E_{\min}, E_{\max}]$ . For a population with spectral index  $\Gamma$  (i.e.,  $F \propto E^{-\Gamma}$ ),  $S$  is related to the differential flux  $F$  by

$$S = F \times \frac{E_{\max}^{1-\Gamma} - E_{\min}^{1-\Gamma}}{(1-\Gamma) E^{-\Gamma}}. \quad (2.3)$$

Hence, we can extrapolate  $\sim \text{GeV}$  gamma-ray fluxes to their  $\sim \text{PeV}$  neutrino counterparts, and compute the correspondent flux probability distribution. Note that we will assume a single injection spectral index  $\Gamma$  as representative of the whole source population for simplicity. In Sec. 6, we will discuss the systematics incurred by employing such an approximation.

## 2.2 Star-forming galaxy fluxes from the *Herschel* data

Although we have a simple conversion between neutrino and gamma-ray fluxes for hadronic sources, SFGs are barely resolved in gamma rays (cf. e.g. [43–46]). Consequently, their neutrino flux distribution is derived following Ref. [11]. We adopt the *Herschel* infrared (IR) luminosity function,  $\Phi(L_{\text{IR}}, z) = d^2N/(dV(z) d\log_{10} L_{\text{IR}})$  [47], defined for the intrinsic infrared luminosity  $L_{\text{IR}}$  and redshift  $z$ . The IR luminosity function is connected to the gamma-ray luminosity function  $\Phi(L_\gamma, z)$  by an empirical correlation

$$\Phi_\gamma(L_\gamma, z) d\log L_\gamma = \Phi_{\text{IR}}(L_{\text{IR}}, z) d\log L_{\text{IR}}, \quad (2.4)$$

$$L_\gamma(L_{\text{IR}}) = 10^\beta \left( \frac{L_{\text{IR}}}{10^{10} L_{\text{solar}}} \right)^\alpha \times \text{erg s}^{-1}, \quad (2.5)$$

where  $\alpha = 1.17 \pm 6\%$  and  $\beta = 39.28 \pm 0.2\%$  [43]; we will assume the best fit values of the above parameters in the following.

As discussed in Refs. [11, 47], the luminosity function of IR galaxies can be decomposed into luminosity functions for spiral (‘normal’) galaxies (NG), starburst galaxies (SB), and star-forming galaxies hosting an obscured or low-luminosity AGN (SF-AGN). This last subpopulation is further divided into those having an energy spectrum resembling the one of normal galaxies (SF-AGN (NG)) and those more similar to starburst galaxies (SF-AGN (SB)); the redshift evolutions of SF-AGNs is given in Table 2 of Ref. [11]. Moreover, SB-like galaxies usually have a harder spectrum than NGs ( $\Gamma_{\text{SB}} = 2.2$  vs.  $\Gamma_{\text{NG}} \simeq 2.7$ , see Ref. [11, 36] and references therein for more details) and therefore in the following we will only consider SB and SF-AGN (SB) galaxies as main contributors to the high-energy neutrino flux. Since SF-AGNs represent the most abundant sub-class of SFGs, we also computed the flux distribution of SF-AGN (NG) as a cross-check ( $\Gamma_{\text{SF-AGN(NG)}} = 2.7$ ). However we find this subpopulation only produces about 6% of the SFG flux between 20 TeV and 5 PeV, and so they have been neglected in our analyses.

We assumed the energy-dependence of the differential flux as an unbroken power-law  $\propto E^{-\Gamma}$  above 0.6 GeV [11] and do not adopt an high-energy cutoff. We will further discuss the uncertainties on  $\Gamma_{\text{SB}}$  in Sec. 6.

### 2.3 Blazar fluxes from the *Fermi* 2FHL catalogue

As a second class of extragalactic neutrino sources, we rely on the Second Catalog of Hard *Fermi*-LAT Sources (2FHL) which probes energies from 50 GeV to 2 TeV [48]. The 2FHL sources are mostly blazars, specifically BL Lacs. One may justify this claim by extrapolating the observed contributions from different blazar populations at high energy ( $\sim 54\%$  BL Lac and  $\sim 16\%$  other blazar sub-populations [48]) to the unassociated and unresolved sources.

Blazars are expected to generate neutrinos mostly through  $p\gamma$  interactions. However, we still adopt for them  $\kappa = 2$  in Eqn. (2.1) (instead of  $\kappa \leq 2$ ), assuming in this way an optimistic estimation of the blazar neutrino contribution. This overestimate accounts to some extent for uncertainty in  $\Gamma_{\text{BL-Lac}}$  (here assumed to be  $\Gamma_{\text{2FHL}} = 2.5$  [48]) and possible contaminations from other sources, currently unassociated/unresolved in the 2FHL. However, checks with  $\kappa = 1$  were found not to significantly affect the results of this study.

### 2.4 Single source distribution

For a gamma-bright population composed of exactly  $N = \int (dV/dz) \Phi(L_\gamma, z) d \log L_\gamma dz$  sources, the luminosity function is sufficient (under the assumption that these extragalactic sources are isotropically distributed in a comoving cosmological volume element  $dV/dz$ ) to obtain the single source distribution:<sup>1</sup>

$$P_1(L_\gamma, z) = \frac{d^2 N / dz dL_\gamma}{N} = \frac{dV}{dz} \frac{\Phi_\gamma(L_\gamma, z)}{N \ln(10) L_\gamma} . \quad (2.6)$$

We use the Planck+WMAP cosmology ( $h = 0.673$ ,  $\Omega_\Lambda = 0.685$ ,  $\Omega_m = 0.313$ ) in  $dV/dz$  [49].

For a population with a unique, fixed spectral index  $\Gamma$  and photons observed at energy  $E_\gamma$  (i.e. emitted at various energies  $(1+z)E_\gamma$ ), the one-source gamma-ray differential flux distribution is obtained by marginalising away the uncertainties on the  $(L_\gamma, z)$  of the source:

$$P_1(F_\gamma | E_\gamma, \Gamma) = \iint dz dL P_1(F_\gamma, L_\gamma, z | (1+z)E_\gamma, \Gamma) = \int dz \left| \frac{L_{\text{crit}}}{F_\gamma} \right| P_1(L_{\text{crit}}, z) , \quad (2.7)$$

where  $L_{\text{crit}}(F_\gamma, E_\gamma, \Gamma, z)$  is the  $L_\gamma$  value obtained by the inversion of the flux model  $F_\gamma(L_\gamma, \dots)$  in which any attenuation during propagation is neglected. Inserting Eqn. (2.6) then yields

$$P_1(F_\gamma | E_\gamma, \Gamma) = \frac{1}{|F_\gamma|} \int dz \frac{dV}{dz} \frac{\Phi_\gamma(L_{\text{crit}}, z)}{N \ln(10)} . \quad (2.8)$$

For the high-flux tail, with contributions only from the nearby sources, the volume probed is very small and we expect an Euclidean scaling  $F^{-2.5}$ . The resulting  $P_1(F)$  is then a broken power-law, up to corrections due to the redshift evolution of the SFG populations [47], as visible in Figure 1.

<sup>1</sup>Throughout this paper, we denote probability distributions by  $P(\dots)$  and distinguish them using the random variables that they describe, along with subscripts if necessary. Conditional and parameterised distributions are denoted as  $P(\cdot|\cdot)$ . The ‘exception’ to this convention is the Poisson distribution, denoted  $\mathcal{P}(\cdot)$ .

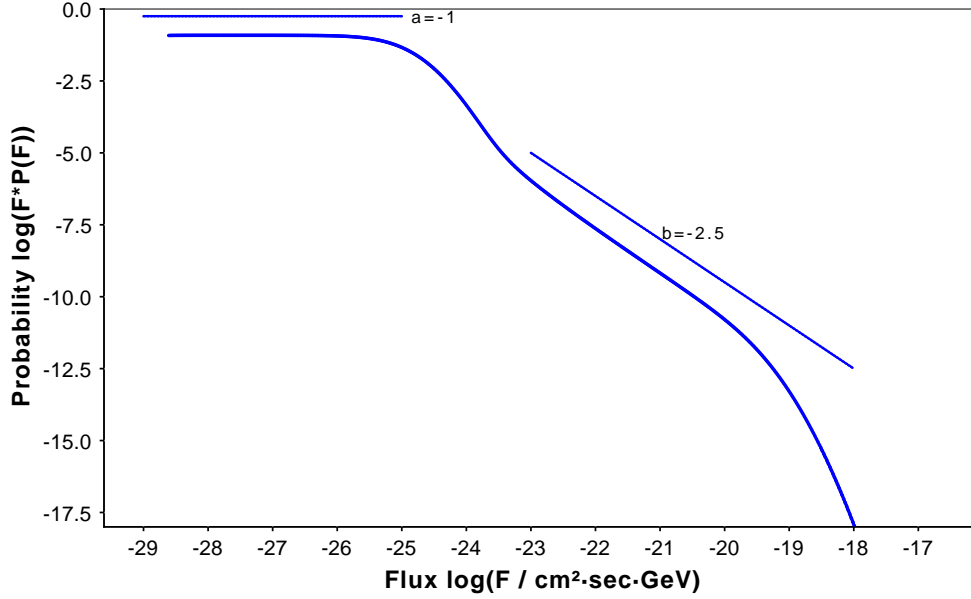


**Figure 1:** Probability distribution  $P_1(F)$  of the differential flux from a single starburst galaxy (SB), obtained by marginalising over the uncertainties on the source intrinsic luminosity and redshift as from Eqn. (2.8). Constant log-slopes corresponding to the limiting  $1/|F|$  and the Euclidean behaviours ( $a$  and  $b$  respectively) are offset and quantified for convenience.

In terms of the number of sources resolved in a flux range  $F \rightarrow F + dF$ , the probability density is

$$P_1(F) = \frac{1}{N} \frac{dN}{dF} . \quad (2.9)$$

Since for any assigned energy spectrum with spectral index  $\Gamma$  we can easily convert  $S \leftrightarrow F$ , we can also take a more direct path from the observed source count distribution  $dN/dS$  to the flux probability distributions. Given a model for the detection efficiency at low fluxes of the instrument generating  $dN/dS$ , one can extrapolate the observed  $dN/dS$  below the detection threshold to obtain the intrinsic  $dN/dS$  (and the total number of sources  $N$  by integration of this quantity). The single-source differential-flux distribution is then simply

$$P_1(F|E, \Gamma) = \frac{\frac{dN}{dS} \frac{dS}{dF}}{N}, \quad (2.10)$$

where the intrinsic  $dN/dS$  is evaluated at  $S = S(F, \Gamma)$  and where  $dS/dF$  is the rightmost term in Eqn. (2.3).

As for the modelling of the 2FHL sources, a Monte-Carlo incorporating the *Fermi* detection efficiency was used in Ref. [50] to obtain the intrinsic  $(dN/dS)_\gamma$ , which we now convert into a neutrino flux distribution assuming  $\kappa = 2$  (cf. Sec. 2.3),  $\Gamma_{\text{BL-Lac}} = 2.5$  [48], and a faintest-source flux cutoff  $S_{\text{min}}$  such as to reproduce the best-fit diffuse flux observed by *Fermi* [50]. This broken power-law flux distribution is a data-driven, phenomenological model of these *Fermi* sources, without any attempt at discriminating subpopulations in the catalog and without consideration of their particular physics.

### 3 Atmospheric foregrounds

Before discussing the flux distributions of the extragalactic astrophysical sources, we introduce the atmospheric foregrounds from which these astrophysical contributions must be extricated [1]. Atmospheric neutrinos produce an almost isotropic foreground with a soft spectrum. Our models of the conventional and prompt contributions are based on Ref. [51] and Ref. [52], respectively. We set the all-flavour neutrino intensity probability density  $P(I_\nu)$ , with  $I_\nu = F_\nu/\Omega$  to Gaussians with finesse  $\mu/\sigma = 10$  (i.e., a 10% intrinsic variability in the atmospheric intensity regardless of pixel size) and with means determined as follows.

For the conventional contribution, the mean intensity is parameterised as

$$\langle I_\nu(E) \rangle = 2 \times 10^{-14} \left( \frac{E}{10 \text{ TeV}} \right)^{-\Gamma_\nu} \text{ cm}^{-2} \text{ s}^{-1} \text{ sr}^{-1} \text{ GeV}^{-1}, \quad (3.1)$$

where the normalisation is set by the  $\nu_\mu$  flux at 10 TeV in Ref. [51] and the extra factor of two accounts for the roughly equal flux of muon anti-neutrinos. For the sake of simplicity, we neglect the anisotropic contributions to the atmospheric flux; for the conventional contribution due to  $\nu_\mu$ , this is mainly a zenith dependence at the South Pole (cf. Fig. 7 in Ref. [51]).

Veto-passing muon events were modelled by rescaling the conventional flux by a factor of 4/3, in accordance with the benchmark event rates from the two-year study which claimed  $\sim 4.5$  and 6 events in  $\nu_\mu$  and  $\mu^\pm$  respectively [1]. The spectrum  $\Gamma_\nu$  is softer than the cosmic ray primaries by  $\Delta\Gamma = 1$ . The cosmic ray knee is shifted down to about 1 PeV for neutrinos, such that

$$\Gamma_\nu(E_\nu) = \begin{cases} 3.7 & \text{when } E_\nu < 1 \text{ PeV} \\ 3.9 & \text{when } E_\nu > 1 \text{ PeV} \end{cases}. \quad (3.2)$$

As for the prompt atmospheric contribution, we interpolate the average  $\nu_\mu + \bar{\nu}_\mu$  flux from Ref. [52] as a function of the energy, and add a rescaling factor of two to account for the roughly equal muon and electron (anti)neutrino fluxes. The enhanced prompt contribution from the proton intrinsic charm [53, 54] is neglected given the opposite shifts in flux from other updated QCD predictions (cf. e.g. [55]), and given the upper limits set in Ref. [4, 56].

The count distribution is then obtained by marginalising the flux distribution into the detector response, with each pixel, energy bin, and event topology treated independently, as will be described in the next section. Convolution of all of these independent distributions gives the predicted distribution of the total number of detected atmospheric neutrinos (and veto-passing muons). The average number of atmospheric counts between 25 TeV and 5 PeV in this model is 27.9. This can be further decomposed into 5.3, 9.7 and 12.9 events from prompt neutrinos, conventional neutrinos, and veto-passing muons, respectively, in rough agreement with an extrapolation of the two-year benchmark rates from Ref. [1] to a four-year lifetime. Poisson shot noise is the dominant source of uncertainty on these event counts, but since we study the fluctuations themselves (statistically), we are in principle sensitive to the assumed  $P(I_\nu)$  rather than just the mean  $\langle I_\nu \rangle$ .

### 4 Flux and count distributions of single pixels

In order to turn the above astrophysical models into predictions about the data observed by IceCube, we must fold in some detector characteristics (angular resolution, effective area, etc.), which will be described in this section. We also derive the total observed flux and count distributions.



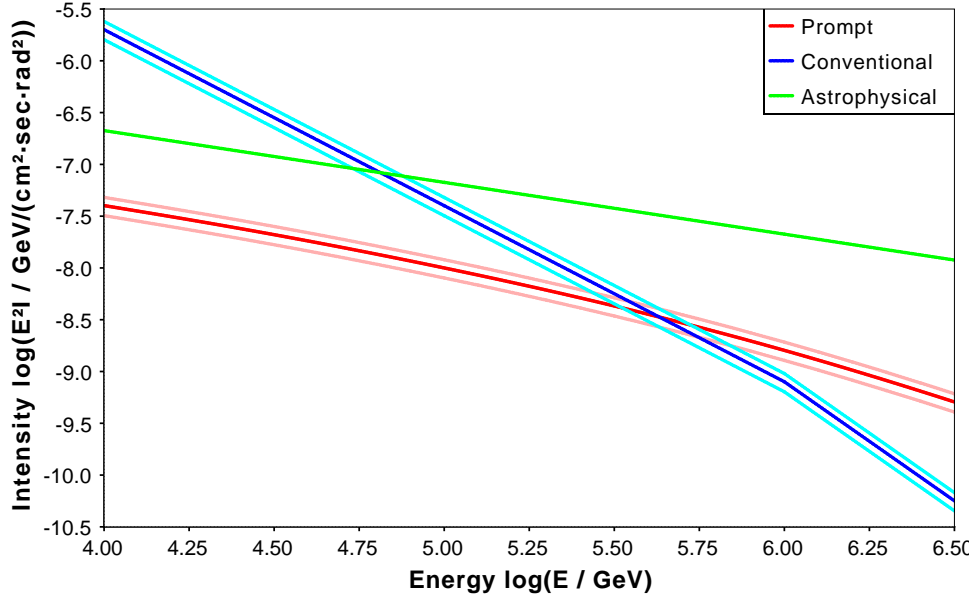


**Figure 2:** Intensity  $E^2 I_\nu(E)$  of the conventional (blue) and prompt (red) atmospheric contributions, as a function of energy. The  $2\sigma$  bands shown here correspond to the  $\sim 10\%$  intrinsic variability of these fluxes assumed in this analysis. These contributions are contrasted to the best-fit flux to the IceCube data from Ref. [57] (green). In addition to these neutrino foregrounds, we also consider the veto-passing muon background (cf. main text).

#### 4.1 Obtaining the total (multi-source) flux distribution

In our analysis, we consider both IceCube tracks and showers (cascades) with pixel exposures constructed from a flavour, energy, and declination dependent effective area tuned to the HESE dataset [1–3]. This dataset consists of 54 events in the energy range [25 TeV, 5 PeV], with interaction vertices contained within the detector: 39 showers, 14 tracks, and one coincident event not used in this analysis.

Since we will be integrating the differential intensities over energies, we will make the simplifying assumption that pixel sizes are constant as a function of the energy: roughly 30 degrees for showers and 1 degree for tracks. These correspond to rough estimates of the median angular resolution of showers [1] and contained tracks [4] at the energies considered in this study (25–5000 TeV). These pixel sizes are used to bin the events into 48 shower pixels and 49152 track pixels, generated using HealPix [58].

We emphasise that the above simplifying assumption is *not* required for a one-point fluctuation analysis: we could generalise this analysis by instead working with pixel sizes constant within any given energy bin but variable across bins at the cost of a greater computational burden. Furthermore, there is no methodological requirement to make pixels of the same scale as the angular resolution; this choice is mostly for ease of comparison with point source search studies in the literature [3, 4, 35, 59] and our forecasts thereof in Sec. 5.1. Note that pixels must be at least as large as the angular resolution in order to treat their fluxes as independent.

The flux incident on a pixel is the sum of the fluxes of all the objects in that pixel. The single-source quantity  $P_1(F)$  therefore needs to be promoted to a multi-source quantity  $P(F)$ . Given the distribution  $P_1(F)$  of the spectral flux per source and the distribution of



the number of sources in a given pixel characterised by the mean  $\langle N' \rangle = (\Omega_{\text{pix}}/4\pi)N$ , it is straightforward to express the distribution  $P(F)$ . By independence of the sources and the algebra of random variables, the distribution of the sum of their fluxes is the auto-convolution

$$P(F|N') = [P_1(F)]^{\star N'} , \quad (4.1)$$

where a further marginalisation over the uncertainty of the number of sources  $N'$  is needed to obtain the unconditional  $P(F)$ .

The marginalised auto-convolution is as difficult to calculate as it is straightforward to express, since the Fourier space techniques usually applied to such compound Poisson distributions [60] develop numerical instabilities for powerlaw-like  $P_1(F)$  spanning many orders of magnitude. We adopt instead the following Monte-Carlo strategy [37]:

- When the average number of sources per pixel  $\langle N' \rangle$  is large, we lump the faint sources into a diffuse Gaussian background and consider only the few brightest sources in that pixel.
- When the average number of (bright) sources per pixel is small, we can repeatedly (i) realise this number  $N'$  from a Poisson distribution with the mean  $\langle N' \rangle$ , (ii) draw that many samples from the single-source flux distribution, and (iii) add them all up. The histogram of the sums of fluxes approximates  $P(F)$ .

In addition, the highest fluxes of  $P(F)$  are known to converge to  $P_1(F)$  [37], which can be used to supplement the MC-derived  $P(F)$  with an analytical “bright point-source” tail. Realising  $N'$  from a Poisson distribution without marginalising over any uncertainties in  $\langle N' \rangle$  effectively suppresses the variance of the statistically isotropic background (cf. Sec. 6), to which one-point methods are sensitive [61, 62].

When the average number of sources per pixel is  $\langle N' \rangle \lesssim 1$ , such as for the 2FHL sources in IceCube track pixels, we encounter the corner case of a flux distribution from zero sources per pixel  $P(F|0) = \delta(F)$ ; we can treat this analytically as

$$P(F) = \sum_{N'=0}^{\infty} \mathcal{P}(N'|\langle N' \rangle) P(F|N') = \exp(-\langle N' \rangle) \delta(F) + \sum_{N'=1}^{\infty} \mathcal{P}(N'|\langle N' \rangle) P(F|N') , \quad (4.2)$$

and choose to sample  $N'$  only from the zero-truncated-Poisson. This trick will become relevant in the next section, when marginalising over fluxes in our detector model to obtain the distribution of the raw data.

## 4.2 Obtaining the observed count distribution

The neutrino fluxes produce discrete event counts in our detector. Having a detector model built into our pipeline means that we can compare the distributional predictions of our astrophysical models directly to the raw event count data (cf. Sec. 5.3 and Sec. 5.4).

At the bare minimum, a detector model  $\mathbf{M}$  consists of a pixel exposure and solid angle. Having already accounted for the latter, the exposure can be constructed by multiplying the IceCube livetime (roughly four years with a 95% duty cycle) by its effective area  $A$ , which is flavour, energy, and declination dependent [1–3]. We postpone discussion of the flavour and declination dependence to the Appendices, and focus here on the energy dependence.

Using Eqn. (2.3) for the conversion from differential fluxes, the flux distribution  $P(S)$  integrated over an energy bin  $[E_{\min}, E_{\max}]$  can be made into a number of counts per pixel and per energy bin, by marginalising the flux distribution into the detector response, as

$$P(C) = \int d\mu \mathcal{P}(C|\mu) P(\mu), \quad P(\mu) = \int \delta(\mu - SAt) P(S) dS = \left. \frac{P(S)}{At} \right|_{S=\mu/At}. \quad (4.3)$$

Assuming independence between multiple energy bins, we can merge bins by convolving the distributions in each bin. Indeed, the total integrated flux  $S$  (respectively the total number of event counts  $C$ ) over a collection of bins is equal to the sum of the integrated fluxes (resp. counts) in each bin. This extensive property of integrated fluxes/counts is useful to account for the fact that the effective area  $A$  is energy-dependent: we can generate  $P(C)$  in some large number of narrow energy sub-bins, where the effective area varies across sub-bins but remains constant inside each one, and then we can convolve the  $P(C)$ 's to merge the sub-bins into a single bin. We refer the interested reader to Appendix A for further discussion of this construction.

As a tradeoff between wanting to exploit the spectrum and hoping to circumvent the low statistics inherent in this endeavour, we generate  $P(C)$  in three final energy bins, with edges at  $[25, 100, 1000, 5000]$  TeV. In the real data, there are 34 events in the 20-100 TeV bin, with a relative Poisson noise of  $\sqrt{34}/34 \sim 17\%$  only marginally larger than that of the full dataset ( $\sqrt{53}/53 \sim 15\%$ ). Of the remaining 19 events, only 3 events lie in the 1-5 PeV bin [3].

Since we are working with relatively wide energy bins, we assume for simplicity that the deposited energy and the neutrino energy are equal, even though this is a poor approximation for tracks; we also neglect uncertainties due to the energy resolution. These are  $\sim 5\%$  and  $\sim 15\%$  systematic and statistical effects, respectively [63]. Our treatment of the anisotropy of the exposure and its dependence on the incident flavour ratio are discussed in Appendices A.2 and A.3.

### 4.3 Distributions of the extragalactic source populations

By applying Eqn. (4.1), we plot in the top panel of Fig. 3 the probability distribution  $P(I)$  of the SFGs at 100 TeV for tracks and showers. Note that the distributions have the form of a Gaussian with a power-law tail. These features correspond to the diffuse glow of a large number of unresolved point sources, and to the few point sources with intensities high enough to be resolved individually [37]. We postpone discussion of point-source-detectability prospects for these populations until Sec. 5.1; here we focus on the physical interpretation and consequences of the features of  $P(F)$ .

Although the single-source flux distribution is independent of the normalisation of the SFG luminosity function, the total flux distribution is sensitive to this normalisation via the average number  $\langle N' \rangle$  of sources per pixel. The uncertainties on normalisations of the SB and SF-AGN (SB) luminosity functions are at the percent-level [47], and thus, are not considered in this study.

The mean and variance of  $P(F)$  are nothing other than a linear rescaling of the mean and variance of  $P_1(F)$  by a factor of  $\langle N' \rangle$ . Moreover, we expect that the peak finesse increases with  $\langle N' \rangle$  (as a consequence of the  $\sqrt{\langle N' \rangle}$  scaling of the finesse in the central limit theorem that gives the diffuse peak its Gaussian shape [37]). This can be corroborated by looking, in Fig. 3 or in Table 1, at the same populations in tracks and in showers: tracks have a better angular resolution and therefore wider diffuse peaks because  $\langle N' \rangle$  drops from  $\mathcal{O}(10^6)$

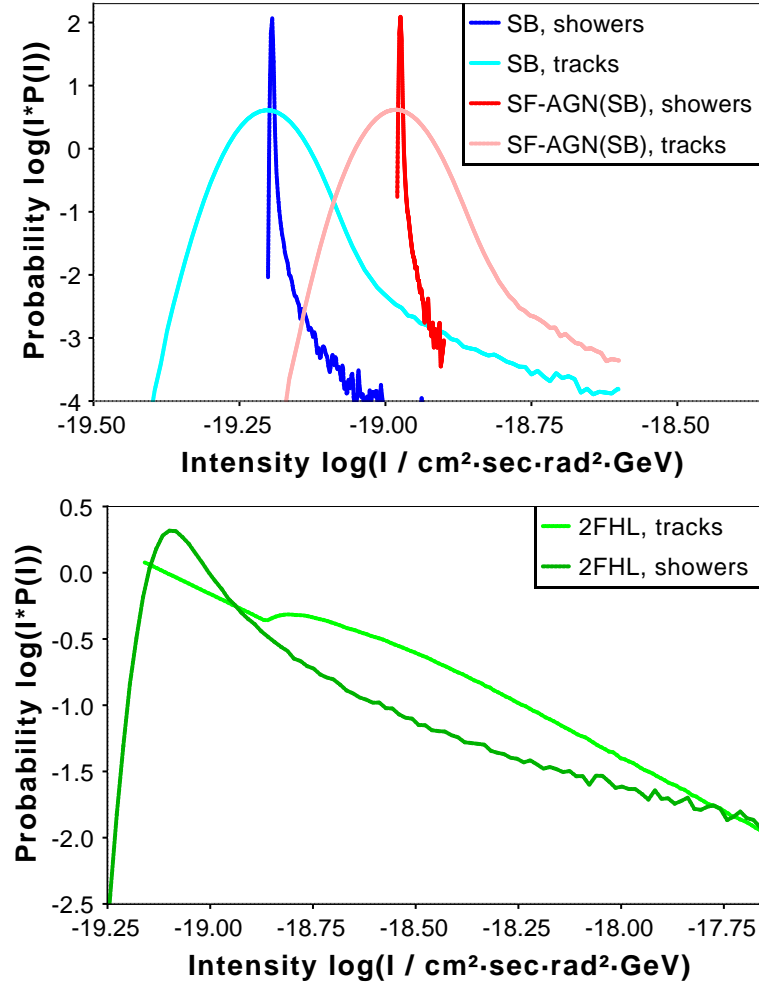


**Figure 3:** *top:* Probability distribution  $P(I)$  of the SFG intensities as observable at 100 TeV. These distributions take the form of a Gaussian peak with a power-law tail. Starbursts are shown in blue (showers) and cyan (tracks), while SF-AGN (SB) are shown in red (showers) and pink (tracks). In each subpopulation, these peaks are much thinner in showers than in tracks as a consequence of the increased number of sources in larger pixels (cf. main text). *bottom:* Probability distribution  $P(I)$  of 2FHL source intensities at 100 TeV, in showers (dark green) and tracks (light green). These distributions are shown conditioned on there actually being a blazar in the pixel, so the absolute and relative normalisations are not visible in this figure. The cusp in tracks occurs at twice the minimum flux, it is the transition from one to two sources per pixel.

to  $\mathcal{O}(10^3)$  in both SB and SF-AGN (SB). A linear regression of the finesse of diffuse peaks from the four  $P(F)$  distributions of SB and SF-AGN (SB) in tracks and showers on their respective  $\sqrt{\langle N' \rangle}$  yields a Pearson  $R^2 = 0.999$ .

The locations of the peaks of these distributions are also slightly offset among each other, the peak in showers is at slightly higher flux than the peak in tracks (again, as visible in Fig. 3 or in Table 1). This is also a consequence of convergence in the central limit theorem. Indeed, the single-source distribution is power-law like and hence very skewed, but the more

sources we have in our pixel, the less we are dominated by the individual source properties and the closer we get to the population mean intensity—which is a quantity dependent on the luminosity function, but independent on the angular resolution. Since showers contain more unresolved sources than tracks, the diffuse peak in showers is closer to the mean of these distributions than the diffuse peak in tracks.

The flux distribution for 2FHL sources in showers (bottom panel of Fig. 3) is qualitatively similar to the flux distributions of SFGs (top panel of the same figure), though its power-law tail is much more prevalent; there are few enough sources per pixel ( $\langle N' \rangle = 429$ ) that even the diffuse peak is distinctly skewed. This non-Gaussianity can, in principle, be exploited to characterise diffuse backgrounds from unresolved sources, even though source number density and source luminosity are degenerate at the level of averages [35]. The small number of sources per pixel also means that the 2FHL peak is much wider than the SFG peaks, by a factor exceeding an order of magnitude (cf. Table 1). This further corroborates the theoretically expected  $\sqrt{\langle N' \rangle}$  scaling of the finesse.<sup>2</sup>

The 2FHL distribution in tracks is informed by the tiny number of sources per pixel ( $\langle N' \rangle = 0.42$ ) and the sharp cutoff imposed at lower fluxes in the single-source distribution in Sec. 2.4. The cusp in the bottom panel of Fig. 3, located at twice the minimum flux, corresponds to the discrete transition from one to two sources per pixel, and below this cusp the distribution is accordingly a pure power-law (corresponding to a single source). Above this cusp, multiple sources contribute jointly to the flux, and a smooth bump begins to form. The power-law tail sets in at higher flux when one of the blazars dominates the flux of the others. As in the case of SFGs, the most likely flux for tracks is still at smaller flux than for showers.

The count distributions  $P(C)$  for our extragalactic sources are, in first approximation, Poisson distributions with means determined by the “diffuse peak” of  $P(F)$ , and the energy/declination-dependent effective area in that pixel. Given the significant tail of  $P(F)$ , the distribution has a skew, such that the location of the peak and the location of the mean do not coincide. When we observe the sky, our observation of event counts is biased by this skewness, as we are more likely to observe the most probable number of counts than the mean number. As discussed above, this bias is increasingly prominent as the pixel size decreases or as the unresolved sources become rarer. While this effect is at the percent-level for SFGs, the mean and mode of  $P(F)$  differ for 2FHL sources by factors of 0.4 in showers and 6.7 in tracks, significantly reducing their anticipated count yield despite not affecting their mean count yield. Amongst other things, this weakens upper limits determined from the population-average contributions of these sources to the diffuse flux (cf. Appendix B for an illustration of this effect). Such a weakening of upper limits derived using averages has been also discussed in the context of dark matter constraints from the diffuse gamma-ray background [37].

Knowledge of the total distribution  $P(F)$  is, however, not necessary to get a good approximation when sources are sufficiently rare. For example, Ref. [64] uses the blazar source count distribution  $dN/dF \propto P_1(F)$  to derive its limits which (as a consequence of  $\langle N' \rangle = 0.42$ ) is a good approximation to the full  $P(F)$  in tracks: the 20% upper limit on the blazar contribution derived therein is not affected by this skewness. Note however that the

---

<sup>2</sup>Although this scaling is a useful tool within a single population of unresolved sources, across multiple source populations other population-specific factors come into play. Indeed, including SF-AGN (NG) in tracks and showers, and 2FHL in showers shows that  $\sqrt{\langle N' \rangle}$  scaling only explains a fraction  $R^2 = 0.79$  of the variance in finesses of these “observations.”

stacking procedure in Ref. [64] increases the effective  $\langle N' \rangle$  in the stacked pixel and thereby deteriorates the quality of this approximation, see also our discussion in Sec. 5.1. On the other hand, because SFGs are so abundant, the average-derived limits on SFG contributions [36] are only a few percents weaker due to this effect—but the fact that these studies do not suffer from this bias could not have been made without using  $P(F)$ .

The reduction in the anticipated number of counts is automatically accounted for by using the full  $P(C)$  rather than the average  $\langle C \rangle$  of source populations in the one-point fluctuation analyses of the next section. In our analysis the full Eqn. (4.3) is used, and the expected number of counts  $\langle C \rangle$ , cumulative over all energies and declinations, in both tracks and showers, is then 2.2 events for SFGs and 2.3 events for 2FHL sources. After subtracting the 28 atmospheric events predicted by our atmospheric model from the 53 actually observed, one expects roughly 25 of these events to be of astrophysical origin. Hence, the expected contributions from SFG and from 2FHL models are each about 10% of the astrophysical flux, well below known upper limits [36, 64], but leaving about 20 events unexplained. The statistical significance with which we can say our model is incomplete (amongst other things we can learn from one-point functions) will be investigated in the next section.

## 5 Results

Given the limited neutrino dataset, the relatively simple models adopted for the different populations, and all the caveats to be specified in Sec. 6, we invite the reader to think of the following exploratory analyses in the spirit of a “model-dependent proof of concept.” In this section, we discuss the possibility of resolving single point sources by applying the statistical tools introduced in the previous sections and we perform various one-point probability distribution analyses.

A few cautionary words about statistical significances [65]: the distributions of the test statistics employed are non-parametric, and we find empirically that they are asymmetric. Therefore we follow the prescription in Ref. [66] and report the one-sided  $p$ -value along with the direction it deviates from the bulk of the distribution of the test statistic. Where appropriate, we correct for the look-elsewhere effect with trial factors, or quote the uncertainty on the  $p$ -statistic due to the finite number of Monte-Carlo realisations used to compute them. Although we do so at times out of convenience to the reader, we recommend against converting these directed- $p$ -values into Gaussian “ $\sigma$ ”s, since ignoring the  $p$ -value from the other tail would artificially inflate this significance and estimating it is error-prone [66].<sup>3</sup>

### 5.1 Resolvability of point sources

Let us consider the ideal limit of a telescope with fixed angular resolution but infinite exposure. The Poisson noise in such an instrument would be negligible, as it would be sensitive to  $P(F)$  directly rather than  $P(C)$ . Even in this idealised situation, the finite angular size of a pixel means that not all sources can be individually resolved: the diffuse peak due to unresolved sources of a given population is then an intrinsic background to point sources of the same population—the only background for such an ideal telescope. In what follows, we argue that even an ideal detector with the IceCube angular resolution would be extremely unlikely to detect SFGs as point sources.

---

<sup>3</sup>This is particularly true for the lower “tail” of our clustering statistic (cf. Fig. 5), for which no such  $p$ -value exists.

**Table 1:** Parameters of the diffuse astrophysical neutrino flux peaks, in units of  $10^{-20} \text{ cm}^{-2} \text{ s}^{-1} \text{ sr}^{-1} \text{ GeV}^{-1}$  and at 100 TeV. Note that the mean contribution  $\hat{\mu}$  in each population is slightly larger for showers than tracks, while the standard deviation  $\hat{\sigma}$  in tracks is wider than showers, as discussed in Sec. 4.3. The  $3\sigma$  and  $5\sigma$  self-background exceedance probabilities per pixel for each subpopulation are also reported.

	Showers $(\theta \sim 30^\circ, N_{\text{pix}} = 48)$			
Population	$\hat{\mu}$	$\hat{\sigma}$	$> 3\sigma$	$> 5\sigma$
2FHL	7.86	0.65	41%	31%
SF-AGN (SB)	10.61	0.024	10%	1.5%
SB	6.40	0.016	6.7%	1.1%
(All)	24.87	0.65		
	Tracks $(\theta \sim 1^\circ, N_{\text{pix}} \sim 5 \times 10^4)$			
Population	$\hat{\mu}$	$\hat{\sigma}$	$> 3\sigma$	$> 5\sigma$
SF-AGN (SB)	10.33	0.84	2.5%	0.25%
SB	6.15	0.48	4%	0.4%
(All)	16.48	0.97		

A point source is basically a localised flux observed in excess of a predetermined threshold value  $F^{\text{pt}}$ . The probability that such a localised excess can be found in any single pixel is given by the exceedance (complementary cumulative) distribution of  $P(F)$ , and the typical number of excesses we expect to see in  $N_{\text{pix}}$  pixels is

$$N_{\text{pt}}(F^{\text{pt}}) = N_{\text{pix}} \int_{F^{\text{pt}}}^{+\infty} P(F) dF \approx N_{\text{pix}} \frac{N(F > F^{\text{pt}})}{N_{\text{MC}}}, \quad (5.1)$$

where the latter has been obtained by estimating the exceedance probability by Monte-Carlo sampling from  $P(F)$ . We recall that  $N_{\text{pix}} \sim 48$  for showers and  $N_{\text{pix}} = 5 \times 10^4$  for tracks.

Because of the sampling rates, this ratio will be most accurate for thresholds placed between the diffuse peak and the power-law tail, i.e., the region where multiple bright sources jointly contribute to the flux and might be confused for a single point source. An analytic approximation to the exceedance probability, valid in the high flux power-law tail where a single source dominates the flux in the pixel, was derived in Ref. [37]. When this approximation matches the Monte-Carlo estimation above, we can be relatively confident that the localised excesses correspond to single astrophysical objects. Hence it is possible to compute the false-positive rate associated to point-source detection with a chosen threshold  $F^{\text{pt}}$ . Because of this possible confusion, the number of localised excesses is always greater than the number of astrophysical point sources. Using localised excesses to determine upper limits for the detection of astrophysical sources is therefore conservative. Also note that stacked searches are intrinsically looking for such localised excesses rather than individual point sources.

We characterise the diffuse peak in terms of a Gaussian as follows: we again take the samples drawn from  $P(F)$  used to estimate Eqn. (5.1), and censor the values above the peak of the distribution where non-Gaussianities due to the power-law nature of the single-source distributions might arise. We then fit the samples below the peak to a doubly truncated

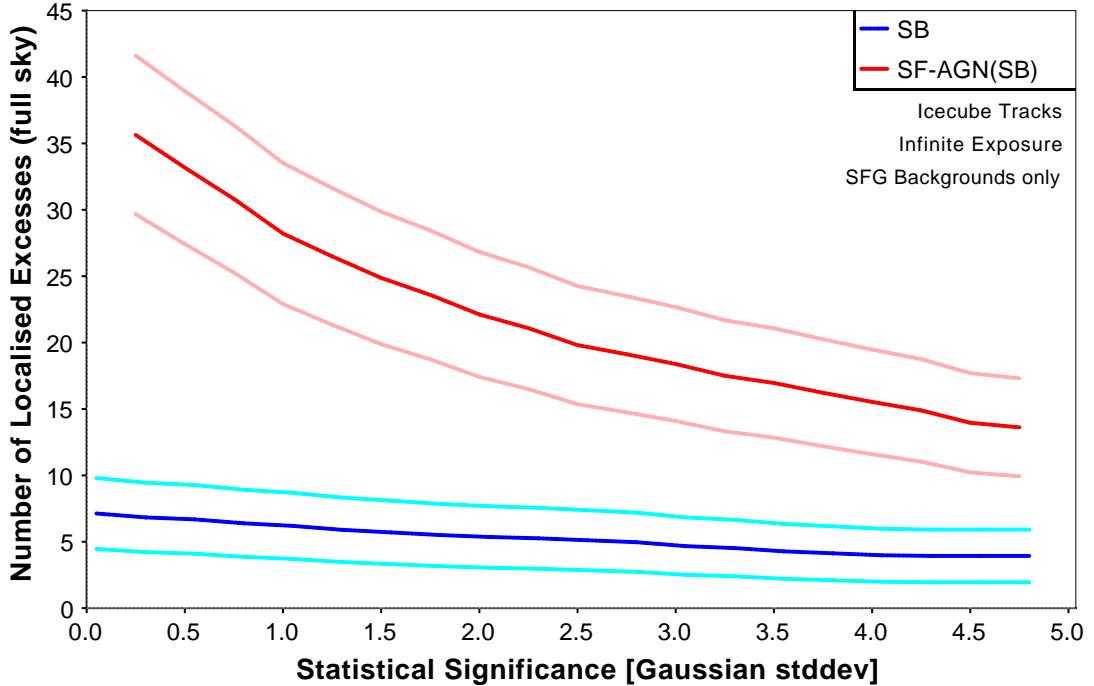


**Figure 4:** Point-source detection prospects ( $N_{\text{pt}}$  vs  $N_{\sigma}$ ) for SB (blue) and SF-AGN (SB) (red) in tracks assuming infinite exposure, IceCube angular resolution, and no backgrounds other than the self-background from SFGs themselves. Poisson error bands on  $N_{\text{pt}}$  are given. These detection prospects are thus intrinsic and conservative upper limits.

normal distribution using the maximum likelihood estimators derived in Ref. [67].<sup>4</sup> The estimated mean and standard deviation of the peak of each population (reported in Table 1) can then be used to define flux thresholds  $F^{\text{pt}}$  for localised excesses  $3\sigma$ ,  $5\sigma$ , etc., above the diffuse peak, and thereby probabilities of observing localised excesses with signal-to-noise ratios of 3, 5, etc., in a given pixel (also in Table 1). These are larger than the exceedance probabilities for a Gaussian ( $\sim 0.1\%$  and  $3 \times 10^{-7}$  at 3 and 5 sigma) because  $P(F)$  is skewed.

## 5.2 Detectability of star-forming galaxies and blazars as point sources

The diffuse backgrounds of unresolved sources are an intrinsic and inescapable feature of any abundant astrophysical population observed with low angular resolution, but population self-backgrounds are not the end of the story. Indeed, sources visible over the *total* astrophysical diffuse flux need to be far brighter and, because flux distribution tails are powerlaw-like, such bright sources are typically rather rare. The expected number of SFG localised excesses resolvable by a detector with an infinite exposure and with the IceCube angular resolution are illustrated in Fig 4. The fluctuations around this expected number are assumed to be Poissonian (also in the following).

In showers, our model of the astrophysical diffuse flux is due to the combination of diffuse fluxes from SB, SF-AGN (SB), and 2FHL sources, i.e., excluding un-modeled populations

<sup>4</sup>Our truncation points are (i) the flux at which the distribution peaks, and (ii) a flux of  $F = 0$ . We still determine  $\hat{\mu}$  from the Monte Carlo samples for the sake of self-consistency, in case the truncation point (derived from an interpolation of the samples) is not exactly at the distribution peak. See Sec. 6 for a discussion of effects that contribute to producing a non-Gaussian diffuse peak.



of neutrino sources. The expected number of  $1\sigma$  excesses over this background is  $N_{\text{pt}} = 6.7 \times 10^{-5}$  for SF-AGN (SB), and similarly we expect  $N_{\text{pt}} = 6.2 \times 10^{-6}$  SB excesses at  $0.1\sigma$ . We conclude that it is unlikely that IceCube would see any significant neutrino excess in showers caused by SFGs, even with an infinite exposure. They are an intrinsically diffuse background with  $30^\circ$  pixels.

On the other hand, we still expect on average  $N_{\text{pt}} = 4 \pm 2$  sources from the 2FHL model above the  $5\sigma$  threshold of the total diffuse extragalactic background at 100 TeV. Although this model does not necessarily rule out associations between single high-energy showers and individual blazars [68–70], it does place an upper limit ( $N_{\text{pt}}$ ) on the number of blazar associations we should expect to corroborate by accumulating more shower data, though this upper limit does not account for the atmospheric backgrounds or shot noise in IceCube. The number of plausible associations with SFGs [71, 72] is similarly bounded from above; However, we should not expect for these sources any corroboration of claimed associations with future data.

The situation in tracks is quite different. As discussed in Sec. 4.3, essentially none of the 2FHL sources contribute to their own diffuse background, and there are roughly 1000 times as many pixels in which to look for excesses. All of the modeled 2FHL sources are resolvable as localised excesses in our infinite-exposure detector. This does not, however, mean that they can all be resolved as individual objects given the backgrounds and shot noise in IceCube. Also, this does not even guarantee a statistical detection of these sources. Indeed, when stacking the  $1^\circ \times 1^\circ$  muon tracks of  $\sim 900$  potential blazar sources in the 2LAC catalogue [64], the effective pixel size is similar to that of a  $30^\circ \times 30^\circ$  shower, and so the effective  $P(F)$  of the stack resembles that of a single shower pixel, the self-background effect becoming relevant again.

Treating all blazars as resolvable point sources, the diffuse background to SB and SF-AGN (SB) then consists in this model of only the joint diffuse flux from SB and SF-AGN (SB) themselves. The number of localised excesses above the diffuse background of all SFGs at 100 TeV is  $N_{\text{pt}} = 17.8 \pm 4.2$  for SF-AGN (SB) and  $N_{\text{pt}} = 4.9 \pm 2.2$  for SB for a  $3\sigma$  threshold (cf. Fig. 4). Even then, these point sources must also be extracted from the background of other (unmodeled) extragalactic contributions, and the atmospheric foregrounds, which in our model shine an order of magnitude brighter than all SFGs combined at 100 TeV.

These non-detectability claims are model dependent, but finite detector exposures and discrete neutrino events would further deteriorate the point-source detection prospects. The SFG non-detectability in IceCube should be expected also from similar studies in gamma-rays: A one-point-fluctuation study of Monte-Carlo simulations of unresolved blazars and SFGs in *Fermi* (which has an angular resolution comparable to that of IceCube tracks) finds that blazars are fitted by a diffuse unresolved point source template, while SFGs are absorbed into a diffuse isotropic template [41].

In short, our model makes two predictions due to self-backgrounds effects. Firstly, SFGs constitute a diffuse background in showers. Secondly, the detectability for SFGs in tracks is very poor: we might see  $N_{\text{pt}} \sim \mathcal{O}(20)$  out of the  $N_{\text{tot}} \sim \mathcal{O}(10^8)$  sources predicted from *Herschel* SB and SF-AGN (SB) luminosity functions, and this prediction needs to be further tempered by unaccounted-for extraterrestrial and atmospheric backgrounds and the finite IceCube exposure.

In the light of these results, we draw attention to the SFG cross-correlation programme pursued in the literature [71, 73, 74]. We have quantitatively shown that SFGs are most probably incapable of acting as localised excesses in IceCube, even if access to far more data than

currently available were possible. A cross-correlation of IceCube data with SFG catalogues, which relies on such excesses, is essentially guaranteed to produce a null result (except when a significant correlation is spuriously driven by fluctuations or non-SFG contaminations). This is consistent with the null [4, 59, 73] or statistically insignificant ( $p \sim 0.3\text{--}0.5$  post-trials [74]) results obtained when attempting to correlate these high-energy events with SFGs.

Since our prediction of a null result is a function of the number of SFGs per pixel, the only way around such negative predictions is to wait for large quantities of data from a neutrino telescope with an angular resolution significantly better than the  $\sim 1^\circ$  achieved in IceCube tracks.<sup>5</sup> Sub-degree angular resolutions for tracks, as expected, e.g., for KM3NeT (ARCA) [75], may allow the nearest SFG point sources to be detected [72]. However, the Galactic foregrounds for such a detection in ARCA will be significant; and note also that stacking the pixels of prospective SFG sources (as discussed in Ref. [35]) increases the effective pixel size, exacerbating this self-background effect (as discussed for blazars above).

### 5.3 A “pointless” clustering analysis

The IceCube collaboration has found no evidence for clustering by looking for hot spots consistent with point sources [3, 4]. But resolving point sources is not the only way we might see clusters of events: in a detector with realistic exposure we can also exploit the statistical properties of localised event clusters due to multiple bright but unresolved sources or even shot noise fluctuations.

Given a fixed pixel size, the one-point function is the most straightforward tool to study neutrino clustering. Indeed, we can directly consider the “average number of clustered neutrinos per pixel” or the “rarity of a cluster of  $N \geq 2$  or more events,”

$$\langle C \geq 2 \rangle = \sum_{C=2}^{\infty} C P(C), \quad \mathfrak{C}(N) = \sum_{C=N}^{\infty} P(C). \quad (5.2)$$

In the ideal case that the data reproduce exactly a Poisson distribution with a mean  $\mu$ , it is easy to show, e.g., that  $\langle C \geq 2 \rangle = \mu(1 - e^{-\mu})$ . However, not only the naïve analysis above would not account for the different angular resolution of tracks and showers and the anisotropic exposure, it would also eschew distributional information by using a single  $\mu$  value rather than the full  $P(\mu)$  from Eqn. (4.3). One should expect two effects to emerge from the power-law tails of astrophysical contributions: on one hand, this tail increases the number of clustered events; on the other hand, this tail contributes a skewness that pushes the most likely values of the distribution to lower flux, as part of a distribution with a fixed mean, resulting (after marginalisation) in less event clustering overall [37].

To go beyond the mean values, let us consider the following per-pixel ( $p$ ) clustering statistic with a model-dependence  $\mathbf{M}$  on the flux distributions and the detector response from Sec. 4:

$$\mathfrak{C}^{(p)} = \begin{cases} \sum_{C=d^{(p)}}^{\infty} P(C|\mathbf{M}) & \text{if } d^{(p)} \geq 2 \\ 1 & \text{otherwise} \end{cases}. \quad (5.3)$$

The total amount of clustering associated to a dataset  $\{\forall p, d^{(p)}\}$  is then quantified by  $\mathfrak{C} = \prod_p \mathfrak{C}^{(p)}$ , and data sets with more clustering (given the same  $P(C|\mathbf{M})$ ) will have a larger

---

<sup>5</sup>Note that the point-source detection prospects forecasted in [72], in which psf-smoothed samples of  $P_1(C) \sim \delta(C - L_{\text{eff}}(z)n_s \times \text{constant exposure})$  for a single population of sources describing all cosmic ray accelerators were used to approximate samples of  $P(C)$ , illustrate (qualitatively) how self-backgrounds decrease with the angular resolution also in detectors with finite exposure.

$-\ln \mathfrak{C}$ . Since we care only about directional information in this test statistic, we need to treat coincident neutrinos of different energies as members of the same cluster. To do so, we follow the prescription of Sec. 4.2 and convolve the count distributions of different energy bins to produce the  $P(C)$  of Eqn. (5.3). The same logic applies to coincident tracks and showers: accurate track pixels were first coarse-grained into shower-sized pixels (cf. Appendix A.2), and then convolved with the shower pixel covering the same patch of sky.

A clustering analysis using  $\mathfrak{C}$  is in a sense a generalisation of the source-counting method applied to the IceCube data in Ref. [35]. In their analysis, the average number of sources producing  $C \geq 2$  tracks was computed from populations of “effective standard candles,” i.e. populations with a luminosity density  $L_{\nu_\mu}^{\text{eff}}$  fixed to an effective value (as a proxy for the full luminosity function). In our distributional study, the average number of sources producing  $C \geq k$  track or shower events could easily be computed by convolving the detector response (cf. Sec. 4.2) over the single-source distributions of Sec. 2; but this quantity would not fully exploit the clustering statistics when multiple sources are present in the same pixel, which are automatically included in the test statistic  $\mathfrak{C}$ .<sup>6</sup>

Applying Eqn. (5.3) to the 53 observed high energy events,<sup>7</sup> we find  $-\ln \mathfrak{C} = 51.3$  over the full sky. Applying  $\mathfrak{C}$  to mock data generated from  $P(C|\mathbf{M})$  then generates the distribution of this test statistic under the null hypothesis, shown in Figure 5 for  $N_{\text{MC}} = 10^{12}$  mock datasets. We easily see that the model produces far less neutrino clustering than observed (typically  $-\ln \mathfrak{C} \lesssim 25$ ).

Since  $\mathfrak{C} = \prod_p \mathfrak{C}^{(p)}$  is separable, this clustering analysis can be performed on small patches of the sky. We study the Southern and Northern hemispheres ( $\delta \lesssim -20^\circ$ , and symmetrically in the North), plus an equatorial band ( $-20^\circ \lesssim \delta \lesssim 20^\circ$ ), where IceCube effective area is maximised, to study whether the observed clustering is consistent with that predicted by our model. We then have  $-\ln \mathfrak{C}^{(N,E,S)} = (13.8, 2.1, 35.4)$ . In the North, we find that the typical  $-\ln \mathfrak{C}$  is smaller in the mock data than in the real data, i.e., less clustering in the mock than in the real data, but with a small one-sided  $p = 0.12$  ( $\sim 1.1\sigma$ ). At the Equator, we find more clustering in the mock data than in the real ones, but again with a negligible one-sided  $p = 0.25$ .<sup>8</sup>

There is more clustering in the Southern hemisphere of the real IceCube data than our model could predict: our knowledge of the significance is in this case limited by the number of Monte-Carlo realisations to the upper bound  $p < 3 \times 10^{-7}$  (one-sided, post-trials). This is roughly equivalent to a  $4.9\sigma$  lower limit on the significance. This discrepancy between our model clustering predictions in the North and its underestimated predictions in the South is *not* an observation of astrophysical anisotropy. IceCube has a higher exposure in the Northern Hemisphere, so we expect a larger number of counts there than in the South; and therefore expect that with the larger Poisson errors associated to this larger number of counts, the North is more tolerant of mis-specification than the South (even though all the contributions to this flux are isotropic). This interpretation is consistent with the even less significant  $p$ -value in the equatorial band, where the exposure is maximised and Poisson errors are largest.

<sup>6</sup>The number of sources contributing  $k$  events is the quantity estimated in one-point fitting studies, which use probability-generating functions to disentangle numbers of clusters into numbers of sources.

<sup>7</sup>The coincident event (#32) has no directional information and was not used in this analysis.

<sup>8</sup>The limited number of distinct mock datasets we can generate with eight pixels in the equatorial declination band discretises the support for the distribution of  $\mathfrak{C}^{(E)}$ . This in turn generates the bin-height alternation in the full-sky distribution of Fig. 5, particularly prominent in the left-hand tail.

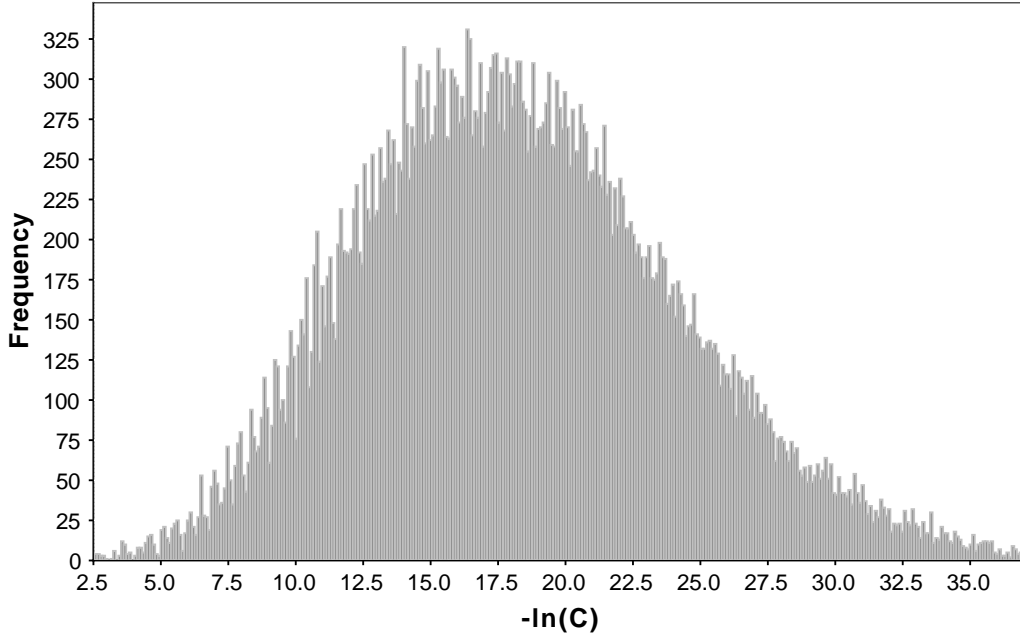


**Figure 5:** Null distribution for  $-\ln \mathfrak{C}$  applied to full-sky mock datasets drawn from our model (including atmospheric foregrounds, unresolved SFG and 2FHL point sources, and anisotropic energy-dependent exposure). The regular, discrete peaks (most prominent at “low clustering”) are due to the finite combinatorics behind producing small amounts of clustering in a finite number of  $30^\circ$  pixels. The value observed in the IceCube data is  $-\ln \mathfrak{C} = 51.3$ .

This interpretation of the discrepancy can be verified by artificially inflating the contribution of extragalactic sources. Let us consider a non-physical model in which SBs are ten times more numerous, for example. The average neutrino flux is then about ten times larger, enough to close the  $\mathcal{O}(20)$  counts gap between the model and the observations. This increase in the SB contribution is found to absorb a significant portion of the Southern discrepancy with only a marginal effect on the North, confirming that we are most sensitive to mis-modelling in the patches of sky with the lowest exposure.

The result of this clustering analysis is then as follows: our data-driven model of the IceCube flux containing only atmospherics, SFGs, and blazars is insufficient to explain the observed clustering with  $\sim 5\sigma$  significance (using our most sensitive region of interest, post-trials). An additional, un-modelled component is necessary to accurately predict the data.

The easiest way to add a large neutrino flux to the model, would be by considering nearby sources. While Galactic sources are not thought to be able to produce PeV neutrinos, they can certainly generate neutrinos up to energies of a few hundred TeV (see, e.g., Ref. [8] for a summary of upper limits on Galactic contributions). As in the extragalactic case, we should not expect a single contribution to account for the entirety of this flux. Amongst other contributions, a phenomenological cosmic-ray model designed to reconcile *Fermi*, Milagro, and local cosmic-ray data, naturally predicts at least 10–20% of the IceCube flux [7]. Whether the addition of this contribution to the model is sufficient to explain the data is left to future work.

## 5.4 One-point fluctuation analysis

The quantity that we have computed to be compared to the data is the anisotropic and spectral probability distribution of event counts. Since there are very few events in our dataset, a  $\chi^2$  analysis of count histograms (the “historical” way to perform a fluctuation analysis) would be untrustworthy. Here, we opt to work directly with the likelihood of the data. The likelihood per pixel ( $\mathcal{L}_p$ ) is a function of the number of counts in a given pixel  $p$  and in a given energy range  $\Delta E$  [40]. Therefore, the total (binned and marginalised) likelihood of a one-point analysis is:

$$\mathcal{L} = \prod_s^{\text{signal}} \prod_{\Delta E}^{\text{energy bin}} \prod_p^{\text{pixel}} P(C = d^{(s, \Delta E, p)} | \mathbf{M}) , \quad (5.4)$$

under the assumption that all the count data  $d^{(s, \Delta E, p)}$  in each of the pixels, energy bins, and signal types/topologies are mutually independent. If detectors other than IceCube were considered in this analysis, an additional product over independent instruments could also be considered (cf. Appendix C). In order to justify the assumption that signal topologies are independent, we explicitly do not consider the “coincident” event (#32) in this analysis.

One feature of this likelihood is that empty pixels (non-observations) also carry information, and that this information is statistically exploited as we will discuss in the next paragraphs. In addition to tracks and showers, IceCube is in principle sensitive to a number of  $\nu_\tau$ -specific topologies [76]. Events in these signal channels would almost certainly be of astrophysical origin, and the nondetection of these topologies can set strong upper limits on the astrophysical  $\nu_\tau$  flux [77]. However, these unobserved topologies were not considered in our model of the IceCube flavour response (cf. Appendix A.3) and do not contribute to  $\mathcal{L}$ .

The likelihood Eqn. (5.4) allows us to assess the predictive power of a model. Indeed, we can draw from  $P(C | \mathbf{M})$  to generate mock data and the exact distribution of the test statistic  $TS = -2 \ln(\mathcal{L})$  under the null  $\mathbf{M}$ , from which a poorness-of-fit for the likelihood of the real data may be computed as a  $p$ -value.<sup>9</sup> All the isotropic components in this study (atmospheric foregrounds, SB and SF-AGN (SB), and 2FHL) contribute to  $\mathbf{M}$ . We generate mock datasets for each model, and partition the mock datasets into ten subsets to generate the sample mean and standard errors of the  $p$  statistic; any  $p$ -values that are too small to resolve are then quoted as upper limits.<sup>10</sup>

By using  $P(C | \mathbf{M})$  in the likelihood rather than just a Poisson at the mean of  $P(F)$ , we automatically account for the skewness-induced difference between the peak and mean values of the flux discussed in Sec. 4.3. However, this skewness drives our prediction to lower counts, and an interesting effect occurs when not only  $\mathbf{M}$  produces a count distribution per pixel of the form

$$P(C) : \{P(0) \approx 1 - \epsilon ; P(1) \approx \epsilon ; \text{rest} \approx 0\} , \quad (5.5)$$

but also  $\mathbf{M}$  is mis-specified in a way that produces a larger total number of counts than in the real data. The effect of this convergence of features is that the real data can give a

<sup>9</sup>Since this  $TS$  is built from the marginal likelihood, it has no dependence on unknown parameters and there is essentially no distinction between the Fisherian (‘classical’) and Bayesian (‘predictive’)  $p$ -values.

<sup>10</sup>In addition to the Monte-Carlo uncertainties, which can in principle be chosen to be arbitrarily small, the experimental uncertainties in the data (due to the finite energy and angular resolution of IceCube) should generate an uncertain value of  $\mathcal{L}$  and hence uncertain  $p$ -values. Also, since the uncertainties on  $p$  are due to finite number of mock datasets rather than to interesting physics (and since we know the model is incomplete, dismissing issues of coverage) the Feldman-Cousins construction of uncertainty bands [78] was not employed.

**Table 2:** Real/mock shower-data likelihoods and one-sided  $p$ -values (pre-trials) in the Northern and Southern skies and in various energy bands. The model includes atmospheric, SFG, and 2FHL contributions. The discrepancy between the mock and real data is fairly significant, especially in the Southern Hemisphere. For a discussion of high-energy northern showers, see Appendix D.

Energy (TeV)	$-2 \ln \mathcal{L}$ (North)	$p$ (North)	$-2 \ln \mathcal{L}$ (South)	$p$ (South)
20 – 5000	26.2 / $37.2 \pm 10.4$	$0.128 \pm 0.003$	95.7 / $19.1 \pm 9.5$	$p < 10^{-5}$
20 – 100	23.6 / $19.2 \pm 6.9$	$0.245 \pm 0.004$	32.6 / $6.77 \pm 5.68$	$(11.1 \pm 1.1) \times 10^{-5}$
100 – 5000	N/A	N/A	63.1 / $12.4 \pm 7.6$	$(1 \pm 1) \times 10^{-5}$

smaller  $-2 \ln \mathcal{L}$  than any of the mock data generated from  $\mathbf{M}$  itself. This effect can then be used as a diagnostic for models that overpredict the number of counts. In the context of a one-point fluctuation analysis, this could mean overpredicting the mean or most likely (cf. Sec. 4.3) number of counts or overpredicting the amount of clustering, e.g., due to an excess of unresolved point sources.

From the clustering analysis above, we know that the model is insufficient to explain the data. But since the global likelihood (Eqn. (5.4)) is a product of independent single-datum-likelihoods, we can decompose the contributions of subsets of the data to our  $-2 \ln(\mathcal{L})$ , to diagnose what is wrong about the model.

We first decompose the likelihoods into the separate contributions from tracks and showers. The track prediction is dominated by conventional atmospheric neutrinos and veto-passing muons, and is surprisingly satisfactory given how crudely we modelled the atmospheric neutrino contribution, slightly overpredicting the counts with  $p = 0.187 \pm 0.004$  (one-sided). This insignificant  $\sim 0.9\sigma$  overprediction suggests that we understand the Northern hemisphere fairly well. In anticipation of the analysis we will do for showers, breaking down this prediction further yields a one-sided  $p \sim 0.3$  for each intersection of the North/South and high/low energy cuts, except for the low-energy northern tracks where we under-predict the data with  $p = 0.080 \pm 0.003$ . However, even this is as weak as  $p \sim 0.3$  (one-sided) after accounting for the look-elsewhere effect of four trials, reaffirming that our non-fine-tuned model can (roughly) predict the track data. Improving the atmospheric foreground models in an attempt to extract astrophysical information out of these events is beyond the scope of this preliminary analysis. In what follows, only the shower data are studied: tracks are only useful to the extent that they corroborate that the detector modeling and atmospheric models are correct.

The data in the North ( $\delta \geq 20^\circ$ ) appear unspectacular (one-sided  $p = 0.24$  post-trials,  $\sim 0.7\sigma$ ) but the data in the South ( $\delta \leq -20^\circ$ ) are unlikely (one-sided  $p < 2 \times 10^{-5}$  post-trials), if  $\mathbf{M}$  is correct. As discussed in Sec. 5.3, the apparent anisotropy is most likely due to the difference in exposure between the North and the South, our method being most sensitive to mismodelling in the South. We use the mock likelihood effect discussed above to interpret this as evidence that the model is over-predicting the counts in the Northern hemisphere (although not significantly, see also Appendix D) and under-predicting the counts in the Southern hemisphere with  $\sim 4.1\sigma$  significance. We have checked that the overprediction effect tied to Eqn. (5.5) does not decrease the statistical significance our deficit in the South—and even if this effect were present, when corrected for it would only increase the significance of this result. We do not think a better modeling of the sources would improve much, especially



since  $\kappa = 2$  for the 2FHL model was taken as an optimistic value and the SFG model does not have a spectral break at high energies [11]. Fixing either or both of these model shortcomings would decrease the anticipated counts from the model and increase the significance of the discrepancy. Hence, we take this as  $\sim 4\sigma$  evidence that other unmodelled components are necessary to predict the IceCube flux at the highest energies.

The one-point analysis can also be used to “characterise” the missing component to a first approximation. Assuming that the analysis of tracks above has validated the detector and the atmospheric models, this discrepancy is deduced to be astrophysical. A further study of the energy-dependence of this southern discrepancy suggests that the unmodelled contribution is missing both in 25-100 TeV and above 100 TeV (cf. Table 2). For a discussion of the energy dependence in the north, see Appendix D.

Despite consistency with our clustering analysis (cf. Sec. 5.3), we must check whether or not the deficit of showers observed in the South is robust to changes in signal region. We can do so by extending the South to include Equatorial pixels, which have the largest exposure of all declinations and are thus least sensitive to model mis-specification. We find that the Equatorial showers (all energies combined) are under-predicted by mock data, albeit with a marginal significance  $p = 0.061 \pm 0.002$  (one-sided, pre-trials). More importantly, the Extended South (Southern + Equatorial pixels) remains significantly underpredicted, with  $p < 10^{-5}$  at both low and high energies (one-sided, pre-trials). Therefore, our claim that the model is missing a component with high significance is robust to changes of the exact extent of our signal region, both below and above 100 TeV.

In short, our data-driven model of the IceCube flux containing only atmospheric foregrounds, SFGs, and blazars is insufficient to explain the observed fluctuation statistics in showers with a robust  $\sim 4\sigma$  significance. Consistency of the model with track data suggests that additional astrophysical contributions are needed, as does the presence of this discrepancy above energies of 100 TeV.

## 6 Discussion

The results presented above are subject to a number of caveats we intend to discuss in this section. Firstly, the effects of extended sources that could potentially affect our “single pixel” results [37] were not studied. The instrumental point-spread function is also a relevant quantity to consider [40], as is the energy resolution or the difference between deposited and real energy [63], amongst others. All of these shortcomings need to be addressed by (ongoing) methodological efforts.

Secondly, although pixel exposure is treated anisotropically, the incident flux distribution was assumed isotropic. This approximation may be sufficient for studies of unresolved extragalactic sources, but morphological, spectral, and distributional templates will be necessary in the future to consistently account for atmospheric and Galactic contributions. Even for unresolved extragalactic sources, the assumption of isotropy may be too strong, as these sources are only *statistically* isotropic. The statistical clustering of unresolved sources is indeed known to affect the flux distributions, and in this study failing to account for this effect underestimates the non-Gaussianity of the flux distribution [61, 62].

Finally, we rely on the best-fit values of a number of parameters. This results in a likelihood that is partially profiled and partially marginalised, and that may introduce systematics. Most importantly, the neutrino fluxes (and their distributions) were extrapolated to high energies using a single value of the spectral slope  $\Gamma$  per population, rather than



extrapolated with a marginalisation over the intrinsic scatter in  $\Gamma$  observed in each population. The uncertainties on  $\Gamma$  are expected to affect the analysis systematically: consider the spectral flux  $F = F_0 \times (E/E_0)^{-\Gamma}$ , with  $P(F_0|E_0)$  and  $P(\Gamma)$  independent and each approximately Gaussian. It can then be shown that  $F$  is normal-log-normally distributed [79]. Thus, marginalisation over  $\Gamma$  generates additional skewness in  $P(F)$ , which might be used in future studies as a tool for studying unresolved source distributions that would otherwise be treated as Gaussians (cf. Sec. 5.1). However, in this study, keeping  $\Gamma$  as a fixed parameter represents a systematic overestimate of the astrophysical fluxes. It is easiest when estimating this systematic effect to ignore distributions and look only at averages. The mean flux of  $P(F|E)$ , assuming  $\Gamma \sim \mathcal{G}(\langle\Gamma\rangle, \sigma_\Gamma^2)$ , is

$$\langle F \rangle = \langle F_0 \rangle \times \left( \frac{E_0}{E} \right)^{\langle\Gamma\rangle + \sigma_\Gamma^2/2}, \quad (6.1)$$

in terms of the mean  $\langle F_0 \rangle$  of an arbitrary  $P(F_0|E_0)$ . The spectrum in our unmarginalised analysis is therefore systematically harder than the average spectrum of the flux by a term of order  $\Delta\Gamma \sim \sigma_\Gamma^2$ . As a consequence, the predicted contributions of our extragalactic components may be slightly overestimated.

This may be particularly relevant for our phenomenological model of 2FHL sources, where the mixture of source populations yields  $\sigma_\Gamma^2 \gg 0.5$  [48]. Accounting for this effect would presumably increase the significance of the  $\sim 4\sigma$ ,  $5\sigma$  discrepancies encountered in the fluctuation and clustering analyses, but since the marginalisation would also broaden  $P(F)$  the net effect would come from more than just this systematic shift.

Along with these methodological caveats, we also adopt a simplified modeling of the atmospheric foregrounds and include only two extragalactic source families. Other guaranteed sources of extragalactic neutrinos have not been included, such as radio galaxies (e.g., [20]). In this sense, a more systematic study of the model sensitivity to the various astrophysical components and uncertainties would be required. Such a study is left to future work. The present work is only meant to test a novel one-point technique on the simplest data-driven model we could construct.

## 7 Conclusions

In this paper, for the first time, we perform a one-point fluctuation study on the high-energy neutrino data from the IceCube telescope. Such an analysis does not require point sources to be resolved in order to study properties of their population statistically, and, in this sense, it revealed to be intrinsically powerful when applied to contemporary data. Since we aimed to explore the power of the one-point statistical analysis in the context of neutrino astronomy, we relied on a naïve modelling of the high-energy neutrino flux in terms of two main extragalactic components (star-forming galaxies and blazars), besides the atmospheric neutrino flux, and compared our predictions with the IceCube detected flux [3]. The extragalactic neutrino backgrounds have been modeled by adopting multi-wavelength data from *Herschel* for the star-forming galaxy component [47] and from the *Fermi* 2FHL source catalogue for blazars [48, 50]. The proposed statistical method has yielded three main results.

Firstly, we quantified to what extent unresolved star-forming galaxies and blazars constitute *their own background* in dedicated IceCube point source searches. We showed that if the neutrino flux of star-forming galaxies is well predicted from the *Herschel* data, then

star-forming galaxies are likely to remain a diffuse, isotropic and featureless background for IceCube: only the diffuse peak of  $P(F)$  can be probed. Note that our conclusions would be even more drastic if relying on more conservative estimates of the SFG neutrino contribution [34, 36]. This model-dependent claim is unequivocally demonstrated in showers, though in tracks we only place a conservative upper limit on the number of resolvable sources  $N_{\text{SFG}} \lesssim 25$  (a number to be revised downward in future studies due to other backgrounds and limited exposures). Our results are in agreement with the null results of dedicated point-source searches and cross-correlation studies [4, 59, 71, 73, 74]. The opposite is predicted for blazars: if the neutrino flux of this source population is well described by the 2FHL source catalogue, then these sources are rare enough that self-background effects are not relevant in tracks. These results are consistent with one-point fluctuation analyses in gamma-rays [41]. However even for blazars, stacking searches focused on IceCube tracks are also prone to a self-background effect, and we derive an upper limit on the number of showers we should expect to associate to blazars.

Secondly, the astrophysical distributions are found to be non-Gaussian with power-law tails. They are highly skewed, implying that IceCube observations are biased away from the mean. For rare sources, the most likely and mean values are predicted to be significantly different, by relative factors between 0.4 (showers) and 6.7 (tracks) in our blazar model. This weakens any upper limits on blazars based on the expected (mean) contributions of these populations to the isotropic flux in tracks, potentially by half an order of magnitude. The skewness of the star-forming galaxy distributions is much smaller, therefore this effect is only percent-level.

Finally, we have applied one-point fluctuation analyses to neutrino data. We find that blazars, star-forming galaxies and atmospheric foregrounds—all treated as statistically isotropic components—contribute in total to two thirds of the observed events. We conclude with a  $4\text{--}5\sigma$  significance that other astrophysical components are needed to explain the IceCube neutrino flux. The likelihood analysis also indicates that the missing component has a spectrum extending above 100 TeV. Given the power intrinsic in such a method, an extended study which takes into account astrophysical uncertainties as well as further astrophysical sources is mandatory as it will allow convergence (even without the need of more neutrino data) towards a multi-wavelength, data-driven, predictive model of the high-energy neutrino sky.

## Acknowledgments

We thank Daniele Gaggero, Franca Hoffman, Jakob van Santen, and Hannes Zechlin for useful discussions. This work was supported by the Netherlands Organisation for Scientific Research through Vidi grant. IT also acknowledges support from the Knud Højgaard Foundation, the Villum Foundation (Project No. 13164) and the Danish National Research Foundation (DNRF91).

## A Modeling of the IceCube effective area

We want to compute (distributionally) the counts registered in a pixel due to a neutrino intensity  $I = F/\Omega_{\text{pix}}$  incident on the detector. Given the distribution  $P(I|E)$  of the energy-differential intensity  $I(E)$ , and an energy-dependent effective area  $A(E)$ , we want to find the

distribution  $P(\mu)$  of the mean number of counts per pixel,

$$\mu_{\text{per pix}} = \int_{E_{\min}}^{E_{\max}} I(E) \Omega_{\text{pix}} A(E) t dE . \quad (\text{A.1})$$

### A.1 Convolutional integration and neutrino fluxes

We can write the integral above as a Riemann sum, i.e.

$$\mu = \lim_{N \rightarrow \infty} \sum_{i=0}^{N-1} I(E + i\Delta E) A(E + i\Delta E) t \Omega \Delta E , \quad (\text{A.2})$$

where  $\Delta E = (E_{\max} - E_{\min})/N$ . We see that  $\mu$  is a normalised sum  $\mu = (X_0 + X_1 + \dots + X_{N-1})/N$  of an infinite number of random variables  $X \sim I A \Omega t$ , for which we might expect the central limit theorem (CLT) to hold. These  $X_i$  are not identically distributed (so the “classical” CLT does not work) but they are independent, so we might be able to use the Lyapunov CLT [80]. However it is easy to show that this extended CLT does not apply either (the Lyapunov Condition is violated for our power-law tailed distributions  $P(I|E)$ ), i.e. that  $P(\mu)$  need not to be Gaussian. Heuristically, if our Riemann sum is  $\mu \sim (X_0 + X_1 + \dots + X_{N-1})$  then the distribution of this infinite sum is the infinite convolution

$$P(\mu) \sim \lim_{N \rightarrow \infty} \bigstar_{i=0}^{N-1} P(X_i) , \quad (\text{A.3})$$

where we recall that  $P(\dots)$  denotes a probability density function. See Figure 6 for a schematic of this convolution with  $N = 4$ .

Less informally, let  $\mu = \int (X|E) dE$  denote an integrated conditional random variable (the “primitive function” or “antiderivative” of the conditional variable  $X|E \in \mathbb{R}^+$  with respect to the random variable  $E$ ). For our purposes, the probability distribution function of  $E$  need not be specified beyond the fact that two fixed limits of integration  $\mathcal{E}_{\min}$  and  $\mathcal{E}_{\max}$  live within the support of  $P(E)$ . We can then express the distribution function  $P(\mu)$  as

$$P(\mu | \mathcal{E}_{\min} \leq E < \mathcal{E}_{\max}) = \lim_{N \rightarrow \infty} \bigstar_{i=0}^{N-1} \left[ \delta \left( \mu - \sum_{j=0}^{N-1} X_j \right) P(X_i | E = \mathcal{E}_{\min} + i\Delta\mathcal{E}) \right] , \quad (\text{A.4})$$

where  $\Delta\mathcal{E} = (\mathcal{E}_{\max} - \mathcal{E}_{\min})/N$  and where  $\delta(\mu - \sum X)$  enforces the Riemann sum on the independent summands  $X_i$ . This expression of course follows from the marginalisation of

$$P(\mu, X_0, \dots, X_{N-1}) = P(\mu | X_0, \dots, X_{N-1}) P(X_0) \dots P(X_{N-1}), \quad (\text{A.5})$$

with  $P(\mu | X\text{'s}) = \delta(\mu - \sum X)$  and  $N \rightarrow \infty$ . A formal definition and study of this operation (presumably in terms of the Itô-Stratonovic stochastic integral [81]) is left to future work, in what follows we adopt physically motivated assumptions in order to compute it. Also, it will be clearer to condense this limit of many convolutions into the notation

$$P(\mu | \mathcal{E}_{\min} \leq E < \mathcal{E}_{\max}) \equiv \bigstar_{\mathcal{E}_{\min}}^{\mathcal{E}_{\max}} P(X|E) dE . \quad (\text{A.6})$$

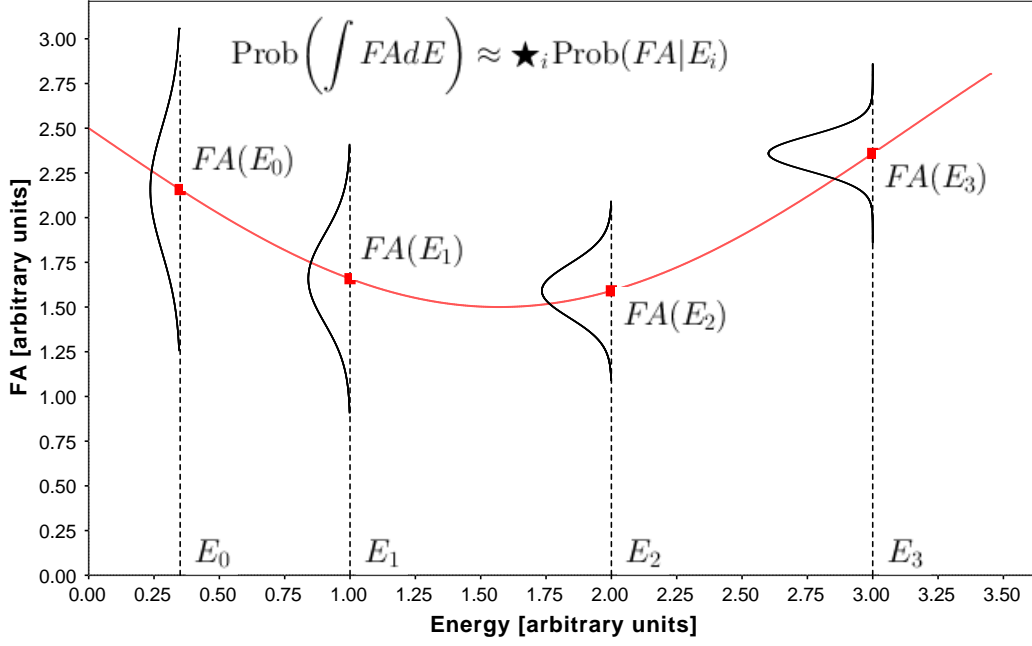


**Figure 6:** Schematic of the integration of a conditional random variable. Specifically, this illustrates the computation of the mean-count distribution  $P(\mu)$ , where  $\mu = \int F A T dE$  with  $T$  constant and  $F = I\Omega$ . Since integrals look like sums, the probability distribution of an integrated quantity is the convolution of the distributions of the integrand as a function of the variable of integration.

Although this quantity is mathematically interesting, in practice we can not compute a number  $N \rightarrow \infty$  of convolutions. Since convolution is associative, convolutive integration is composable in its boundaries:

$$\star_a^c P(F|E)dE = \left( \star_a^b P(F|E)dE \right) \star \left( \star_b^c P(F|E)dE \right). \quad (\text{A.7})$$

Using this property and working with integrated fluxes  $S = \int F dE$ , we can approximate the convolutive integral of differential fluxes as the convolution of integrated fluxes:

$$\star_{\Delta E} P(F|E)dE \approx \star_{i=0}^{N-1} P(S|\delta E_i). \quad (\text{A.8})$$

This *distributionally* reproduces the insight (conveyed in the main text) that the flux  $S$  is an extensive quantity (with respect to  $E$ ), so that the flux over a sum of bins is the sum of the fluxes in each bin  $S(\Delta E) = \sum_i S(\delta E_i)$ . With this understanding, we can finally compute

$$P(\mu|\Delta E) \approx \star_{i=0}^{N-1} P(S_i \times A_i \times t | \delta E_i), \quad (\text{A.9})$$

where the number of convolutions is chosen large enough that  $A(E)$  can be treated as a constant  $A_i$  in each subbin  $\delta E_i$ .

## A.2 Declination dependence

In addition to this energy-dependence, note that the effective area is also declination dependent. In our analysis we simply use the central declination of each pixel to compute  $A(E)$ . For showers, HealPix [58] generates pixels at seven different latitudes, calling for seven computations of  $P(C)$  for each source class, for each of the two event topologies, and for each of the three energy bins. For tracks, HealPix generates 255 different latitudes. To facilitate comparisons we compute  $P(C)$  at the same seven latitudes as for showers and use whichever declination is closest. This is particularly relevant for our discussion of clustering in Sec. 5.3, where the distributions in tracks were coarse-grained to the scale of showers by autoconvolution. This shortcut can only be exploited if we restrict ourselves to components with at most iso-latitudinal variations such as (to a good approximation) the atmospheric component [51]. A dedicated analysis of truly anisotropic components, such as the neutrino contribution of the Galactic plane [7], is left to future work.

## A.3 Flavour dependence

IceCube provides a separate estimation of the effective area for each of the three flavours, which we interpolate in declination and energy in order to use the formalism above. However, the effective area for tracks and showers depends on the probability  $p_{T/S}^{e/\mu/\tau}$  that a neutrino of a given flavour (sampled randomly from the total neutrino flux) produces a charged or a neutral current interaction in the ice. We use the approximation [82]

$$\{p_T^\mu = 0.8, p_S^\mu = 0.2, p_S^{e/\tau} = 1, p_T^{e/\tau} = 0\} \quad (\text{A.10})$$

to write

$$A_{T/S} = 2 \sum_{f \in \{e, \mu, \tau\}} p_{T/S}^f \times A^f \times \eta^f, \quad (\text{A.11})$$

where  $A^f$  is the flavour-energy-and-declination dependent quantity given by IceCube [1] and  $\eta^f$  is the fraction of neutrinos of a given flavour ( $\eta = 1/3$  for a 1 : 1 : 1 flavour ratio). We multiply the effective area by 2 since the sum does not run over antineutrinos, effectively setting equal neutrino and antineutrino fluxes. We employ a 1 : 1 : 1 ratio for all extragalactic components, a 0 : 1 : 0 flavour ratio for the conventional atmospheric flux, and a 1 : 1 : 0 ratio for the prompt atmospheric flux [52]. Percent-level atmospheric contributions from  $\nu_e$  and  $\nu_\tau$  fluxes (respectively) [51, 52] are neglected, as are the neutrino-antineutrino ratios, although the fully detailed (even energy-dependent) flavour ratios can manifestly be accounted for in this type of analysis.

## B Illustration of the bias on the blazar contribution

In Sec. 4.3 we found that the skewness of the blazar  $P(F)$  biases results derived from population means by a non-negligible factor compared to the full distributional result. In this section, we estimate the average fraction of the astrophysical IceCube flux explained by 2FHL sources using a population-average approach, in order to illustrate that this approach yields biased (incorrectly strong) constraints on the blazar contribution in comparison with the  $P(C)$  prediction.

Consider constructing  $dN/dF_\nu$  from the same assumptions that went into the  $P(C)$  prediction that blazars contribute  $\sim 10\%$  of the astrophysical flux observed in IceCube:

1. The total number of sources  $N_\nu = N_\gamma$  is the same, and their  $\gamma$ -ray and  $\nu$  fluxes share a single intrinsic spectrum  $\Gamma = 2.5$ ;
2. The 2FHL sources explain *on average* a fraction  $f$  of the astrophysical flux observed by IceCube

$$\frac{1}{4\pi} \int F_\nu \frac{dN}{dF_\nu} dF_\nu = f \langle I_{\text{IceCube}} \rangle, \quad (\text{B.1})$$

where the best-fit power-law model of this flux is  $\langle I_{\text{IceCube}} \rangle = 6.7^{+1.1}_{-1.2} \cdot 10^{-18} (E/100 \text{ TeV})^{-2.5} \text{ cm}^{-2} \text{ s}^{-1} \text{ sr}^{-1} \text{ GeV}^{-1}$  between 25 TeV and 2.8 PeV [57];

3. The minimum flux  $S_{\text{min},\gamma}$  to which we extrapolate the distribution  $dN/dS_\gamma$  is chosen to reproduce the best-fit *average* diffuse flux observed by *Fermi* between 50 GeV and 2 TeV,  $\langle S_{\text{Fermi}} \rangle = 2.07 \cdot 10^{-9} \text{ cm}^{-2} \text{ s}^{-1} \text{ sr}^{-1}$  [50].

All of the parameters of the neutrino source distribution  $dN/dF_\nu$  may be fixed by these assumptions, up to a degeneracy in the fraction  $\kappa/f$ . Indeed, once  $S_{\text{min}}$  has been fixed by the *Fermi* data, we can compute the number of neutrino sources  $N_\nu$  as an integral over the  $\gamma$ -ray source distribution. We can then convert between  $\gamma$ -ray and  $\nu$  distributions using Eqn. (2.3). Since the slopes below and above the break of  $dN/dS_\gamma$  are  $\alpha = -(1.7^{+0.05}_{-0.1}) > -2$  and  $\beta = -2.5 < -2$  respectively, the majority of the flux comes from the break itself in the Paretian approximation

$$\int F_\nu \frac{dN}{dF_\nu} dF_\nu \sim N \times \frac{\alpha - 1}{F_{\text{min},\nu}^{1-\alpha}} \times \frac{F_{\text{break},\nu}^{2-\alpha}}{2 - \alpha} \sim N \frac{(\alpha - 1)}{(2 - \alpha)} (3\kappa) \frac{F_{\text{break},\gamma}^{2-\alpha}}{F_{\text{min},\gamma}^{1-\alpha}}, \quad (\text{B.2})$$

from which

$$\frac{\kappa}{f} = \frac{4\pi \langle I_{IC} \rangle}{3N} \frac{\alpha - 2}{\alpha - 1} \frac{F_{\text{min},\gamma}^{1-\alpha}}{F_{\text{break},\gamma}^{2-\alpha}} = 109^{+43}_{-26}. \quad (\text{B.3})$$

In our estimation of the uncertainty, we numerically propagate the (upper and lower) uncertainties on  $\langle I_{IC} \rangle$  and  $\alpha$  through the computation above, and add these uncertainties in quadrature. The assumed spectrum  $\Gamma = 2.5$  is equal to that of the fit to the high-energy IceCube data [57], so that  $\kappa/f$  is constant in energy; in general it would be a function of the energy  $\propto E^{\Delta\Gamma}$ . By asserting a value of  $\kappa$ , we can determine  $f$ . Since the blazar neutrino flux mostly originates from  $p\gamma$  interactions, we expect  $\kappa \leq 2$  and that the fraction  $f$  becomes smaller as  $\kappa$  decreases. Within the above uncertainty margin, the upper limit ( $\kappa = 2$ ) on the 2FHL contribution to the (astrophysical) diffuse IceCube flux is  $f = 2.5\%$ .

The upper limit we have just derived could be slightly weakened by the inclusion of other uncertainties ( $\beta$ ,  $\langle S_{\text{Fermi}} \rangle$ , etc.), or strengthened by adopting a more realistic  $\kappa \leq 2$ , but this is clearly a much stronger upper limit than the actual  $\sim 10\%$  contribution predicted using  $P(C)$ . This illustrates that the skewness of the total flux distribution  $P(F)$  introduces a significant bias between the mean contribution and the contribution most likely to be observed in IceCube, which produces a systematic effect on upper limits derived using average quantities (as discussed in Sec. 4.3).

## C Methodological contrast to one-point *fitting*

One-point methods, pioneered and refined by  $P(D)$  analysis [60–62], are currently experiencing a rebirth in contemporary astrophysics [37–41, 83–89]. The objective of such methods

is typically to fit the resolved and unresolved point source distribution  $dN/dF$  to the data in terms of a phenomenological model, to be interpreted after the conclusion of the analysis proper. In gamma-rays, for example, the generating function approach in Ref. [38] was for this purpose considerably enhanced, with careful studies of the  $dN/dF$  prior-dependence [40, 84] and systematics [41] of the fitting procedure. Both the generating-function-fitting method and the distribution-modelling method in the present study essentially require (i) an ansatz on the source count distribution,<sup>11</sup> (ii) a model of the response of the instrument to incident flux, and (iii) a way to transition from one to the other.

The two approaches are most obviously distinguished by this third point, particularly by the direction of this transition (from model to prediction / from data to fit) and by its nature (a probabilistic hierarchical network / use of a specific statistical estimator). A perhaps more subtle distinction between the two methods is that one can model the flux distribution of many source populations in many detectors, while the specific estimator adopted in the fitting method is (at least in its current form) one-to-one. The main text illustrates the multiplicity of source populations, but besides IceCube, all instruments sensitive to high-energy neutrinos currently produce non-measurements [90–92]. And although in this study we restrict our attention to neutrino data at the highest energies, a one-point analysis can in principle be both multi-wavelength and multi-messenger, if the model  $\mathbf{M}$  of astrophysics and of instrument responses that gives rise to the  $P(C|\mathbf{M})$  count distributions is sufficiently elaborate.

In gamma-rays, there is enough data that the choice between the two methods is to a large extent a matter of taste. However, a generating-function analysis would be ill-suited to the low statistics of contemporary high-energy IceCube data: such an analysis is blind to features below the single-event sensitivity [40]. One should expect that the experimental event count distribution is too poorly sampled to drive significant fits of the source count distribution. Even if it were not, it would *by design* be incapable of disentangling the subdominant source population contributions from its unique  $dN/dF$ : any post-hoc interpretation of such a poorly-fit  $dN/dF$  would live in a limbo of untested conjectures in wait of more data.

By contrast, in the modelling approach, various hypothetical combinations of flux distributions can be tested against the neutrino data. When they fail to be rejected by the data, or when preferences between multiple models fail to emerge significantly from the data, this occurs formally and quantifiably. On the other hand, when a model is rejected by the data, and hypotheses for this failure are put forward (in our case, the hypothesis that there is a contribution missing), these are *guaranteed to be testable with contemporary data* (by improvement of the model and re-analysis). These model improvements and tests are not a methodological shortcoming, but indeed an opportunity to be explored in future work.

## D One-point fluctuation analysis: cross checks

In order to more critically assess the significance of our results, we here discuss some limitations of the statistical tools with which our  $p$ -statistics were derived. One of these limitations becomes clear if we continue to narrow our focus on the Northern Hemisphere, and again consider two parts of the data separately: The prediction is rather poor at higher energies, where the model overpredicts the counts ( $-2 \ln \mathcal{L} = 2.7 / 17.95 \pm 7.6$ ) with a significance of  $p < 4 \times 10^{-5}$  post-trials (reported as “N/A” in Table 2). This overprediction persists no

---

<sup>11</sup>In the generating-function approach, this is an ansatz on the parameterisation of  $dN/dF$  and on the priors associated to the parameter values.



**Table 3:** Actual / Mock shower-data likelihoods and one-sided  $p$ -values, in the Northern and Southern skies and in various energy bands. The model considered includes SFG and 2FHL contributions, as well as deliberately mis-specified atmospheric contributions.

Energy (TeV)	$-2 \ln \mathcal{L}$ (North)	$p$ (North)	$-2 \ln \mathcal{L}$ (South)	$p$ (South)
20 – 5000	24 / $36 \pm 10$	$0.096 \pm 0.004$	113 / $13.4 \pm 8$	$< 10^{-4}$
20 – 100	22.1 / $22.7 \pm 7$	$0.382 \pm 0.003$	37.8 / $5.9 \pm 5.3$	$(1 \pm 0.3) \times 10^{-4}$
100 – 5000	1.8 / $13.3 \pm 7.1$	$< 10^{-4}$	74.7 / $7.7 \pm 6.6$	$< 10^{-4}$

matter how many source classes or atmospheric contributions are removed from the model, because we have subdivided the data so much that there is only one shower above 100 TeV in all of the Northern Hemisphere (event #26): we are comparing a  $P(C)$  of the form in Eqn. (5.5) to extremely sparse data, so we observe extreme likelihoods for any model.

Another cross-check we performed was to deliberately mis-specify the flavour ratio of the conventional and prompt atmospheric fluxes; 1 : 4 : 0 was used, appropriate only for energies  $E_\nu \sim 30$  GeV [51] (three orders of magnitude below the lowest energies considered in this analysis). The effect of this change in showers was mild (see Table 3). The North/South feature discussed in the main analysis is still present, as is the overprediction effect in high-energy northern showers. This mis-specification had no effect on the clustering analysis of Sec. 5.3, as expected since only information regarding direction of arrival was used in that analysis.

## References

- [1] **IceCube** Collaboration, M. G. Aartsen et al., *Evidence for High-Energy Extraterrestrial Neutrinos at the IceCube Detector*, *Science* **342** (2013) 1242856, [[arXiv:1311.5238](#)].
- [2] **IceCube** Collaboration, M. G. Aartsen et al., *Observation of High-Energy Astrophysical Neutrinos in Three Years of IceCube Data*, *Phys. Rev. Lett.* **113** (2014) 101101, [[arXiv:1405.5303](#)].
- [3] **IceCube** Collaboration, C. Kopper, W. Giang, N. Kurahashi, et al., *Observation of astrophysical neutrinos in four years of icecube data*, in *PoS (ICRC2015) 1081*, 2015.
- [4] **IceCube** Collaboration, M. G. Aartsen et al., *All-sky search for time-integrated neutrino emission from astrophysical sources with 7 years of IceCube data*, [arXiv:1609.04981](#).
- [5] L. A. Anchordoqui et al., *Cosmic Neutrino Pevatrons: A Brand New Pathway to Astronomy, Astrophysics, and Particle Physics*, *JHEAp* **1-2** (2014) 1–30, [[arXiv:1312.6587](#)].
- [6] A. Neronov and D. V. Semikoz, *Evidence the Galactic contribution to the IceCube astrophysical neutrino flux*, *Astropart. Phys.* **75** (2016) 60–63, [[arXiv:1509.03522](#)].
- [7] D. Gaggero, D. Grasso, A. Marinelli, A. Urbano, and M. Valli, *The gamma-ray and neutrino sky: A consistent picture of Fermi-LAT, Milagro, and IceCube results*, *Astrophys. J.* **815** (2015), no. 2 L25, [[arXiv:1504.00227](#)].
- [8] M. Ahlers and K. Murase, *Probing the Galactic Origin of the IceCube Excess with Gamma-Rays*, *Phys. Rev.* **D90** (2014), no. 2 023010, [[arXiv:1309.4077](#)].
- [9] H.-N. He, T. Wang, Y.-Z. Fan, S.-M. Liu, and D.-M. Wei, *Diffuse PeV neutrino emission from ultraluminous infrared galaxies*, *Phys. Rev.* **D87** (2013), no. 6 063011, [[arXiv:1303.1253](#)].
- [10] R.-Y. Liu, X.-Y. Wang, S. Inoue, R. Crocker, and F. Aharonian, *Diffuse PeV neutrinos from EeV cosmic ray sources: Semirelativistic hypernova remnants in star-forming galaxies*, *Phys. Rev.* **D89** (2014), no. 8 083004, [[arXiv:1310.1263](#)].
- [11] I. Tamborra, S. Ando, and K. Murase, *Star-forming galaxies as the origin of diffuse high-energy backgrounds: Gamma-ray and neutrino connections, and implications for starburst history*, *JCAP* **1409** (2014), no. 09 043, [[arXiv:1404.1189](#)].
- [12] L. A. Anchordoqui, T. C. Paul, L. H. M. da Silva, D. F. Torres, and B. J. Vlcek, *What IceCube data tell us about neutrino emission from star-forming galaxies (so far)*, *Phys. Rev.* **D89** (2014), no. 12 127304, [[arXiv:1405.7648](#)].
- [13] S. Chakraborty and I. Izaguirre, *Diffuse neutrinos from extragalactic supernova remnants: Dominating the 100 TeV IceCube flux*, *Phys. Lett.* **B745** (2015) 35–39, [[arXiv:1501.02615](#)].
- [14] N. Senno, P. Mészáros, K. Murase, P. Baerwald, and M. J. Rees, *Extragalactic star-forming galaxies with hypernovae and supernovae as high-energy neutrino and gamma-ray sources: the case of the 10 TeV neutrino data*, *Astrophys. J.* **806** (2015), no. 1 24, [[arXiv:1501.04934](#)].
- [15] O. E. Kalashev, A. Kusenko, and W. Essey, *PeV neutrinos from intergalactic interactions of cosmic rays emitted by active galactic nuclei*, *Phys. Rev. Lett.* **111** (2013), no. 4 041103, [[arXiv:1303.0300](#)].
- [16] F. W. Stecker, *PeV neutrinos observed by IceCube from cores of active galactic nuclei*, *Phys. Rev.* **D88** (2013), no. 4 047301, [[arXiv:1305.7404](#)].
- [17] K. Murase, Y. Inoue, and C. D. Dermer, *Diffuse Neutrino Intensity from the Inner Jets of Active Galactic Nuclei: Impacts of External Photon Fields and the Blazar Sequence*, *Phys. Rev.* **D90** (2014), no. 2 023007, [[arXiv:1403.4089](#)].
- [18] C. D. Dermer, K. Murase, and Y. Inoue, *Photopion Production in Black-Hole Jets and Flat-Spectrum Radio Quasars as PeV Neutrino Sources*, *JHEAp* **3-4** (2014) 29–40,

- [arXiv:1406.2633].
- [19] P. Padovani, M. Petropoulou, P. Giommi, and E. Resconi, *A simplified view of blazars: the neutrino background*, *Mon. Not. Roy. Astron. Soc.* **452** (2015), no. 2 1877–1887, [arXiv:1506.09135].
  - [20] D. Hooper, *A Case for Radio Galaxies as the Sources of IceCube’s Astrophysical Neutrino Flux*, *Submitted to: JCAP* (2016) [arXiv:1605.06504].
  - [21] K. Murase and J. F. Beacom, *Galaxy Clusters as Reservoirs of Heavy Dark Matter and High-Energy Cosmic Rays: Constraints from Neutrino Observations*, *JCAP* **1302** (2013) 028, [arXiv:1209.0225].
  - [22] F. Zandanel, I. Tamborra, S. Gabici, and S. Ando, *High-energy gamma-ray and neutrino backgrounds from clusters of galaxies and radio constraints*, *Astron. Astrophys.* **578** (2015) A32, [arXiv:1410.8697].
  - [23] K. Murase and K. Ioka, *TeV-PeV Neutrinos from Low-Power Gamma-Ray Burst Jets inside Stars*, *Phys. Rev. Lett.* **111** (2013), no. 12 121102, [arXiv:1306.2274].
  - [24] R.-Y. Liu and X.-Y. Wang, *Diffuse PeV neutrinos from gamma-ray bursts*, *Astrophys. J.* **766** (2013) 73, [arXiv:1212.1260].
  - [25] I. Tamborra and S. Ando, *Diffuse emission of high-energy neutrinos from gamma-ray burst fireballs*, *JCAP* **1509** (2015), no. 09 036, [arXiv:1504.00107].
  - [26] I. Tamborra and S. Ando, *Inspecting the supernova?gamma-ray-burst connection with high-energy neutrinos*, *Phys. Rev.* **D93** (2016), no. 5 053010, [arXiv:1512.01559].
  - [27] N. Senno, K. Murase, and P. Meszaros, *Choked Jets and Low-Luminosity Gamma-Ray Bursts as Hidden Neutrino Sources*, *Phys. Rev.* **D93** (2016), no. 8 083003, [arXiv:1512.08513].
  - [28] Y. Fujita, S. S. Kimura, and K. Murase, *Hadronic origin of multi-TeV gamma rays and neutrinos from low-luminosity active galactic nuclei: Implications of past activities of the Galactic center*, *Phys. Rev.* **D92** (2015), no. 2 023001, [arXiv:1506.05461].
  - [29] S. S. Kimura, K. Murase, and K. Toma, *Neutrino and Cosmic-Ray Emission and Cumulative Background from Radiatively Inefficient Accretion Flows in Low-Luminosity Active Galactic Nuclei*, *Astrophys. J.* **806** (2015) 159, [arXiv:1411.3588].
  - [30] B. Feldstein, A. Kusenko, S. Matsumoto, and T. T. Yanagida, *Neutrinos at IceCube from Heavy Decaying Dark Matter*, *Phys. Rev.* **D88** (2013), no. 1 015004, [arXiv:1303.7320].
  - [31] A. Esmaili and P. D. Serpico, *Are IceCube neutrinos unveiling PeV-scale decaying dark matter?*, *JCAP* **1311** (2013) 054, [arXiv:1308.1105].
  - [32] J. Zavala, *Galactic PeV neutrinos from dark matter annihilation*, *Phys. Rev.* **D89** (2014), no. 12 123516, [arXiv:1404.2932].
  - [33] K. Murase, R. Laha, S. Ando, and M. Ahlers, *Testing the Dark Matter Scenario for PeV Neutrinos Observed in IceCube*, *Phys. Rev. Lett.* **115** (2015), no. 7 071301, [arXiv:1503.04663].
  - [34] S. Ando, I. Tamborra, and F. Zandanel, *Tomographic Constraints on High-Energy Neutrinos of Hadronuclear Origin*, *Phys. Rev. Lett.* **115** (2015), no. 22 221101, [arXiv:1509.02444].
  - [35] K. Murase and E. Waxman, *Constraining High-Energy Cosmic Neutrino Sources: Implications and Prospects*, [arXiv:1607.01601].
  - [36] K. Bechtol, M. Ahlers, M. Di Mauro, M. Ajello, and J. Vandenbroucke, *Evidence against star-forming galaxies as the dominant source of IceCube neutrinos*, [arXiv:1511.00688].
  - [37] M. R. Feyerhisen, S. Ando, and S. K. Lee, *Modelling the flux distribution function of the extragalactic gamma-ray background from dark matter annihilation*, *JCAP* **1509** (2015), no. 09

- 027, [[arXiv:1506.05118](#)].
- [38] D. Malyshev and D. W. Hogg, *Statistics of gamma-ray point sources below the Fermi detection limit*, *Astrophys. J.* **738** (2011) 181, [[arXiv:1104.0010](#)].
  - [39] S. K. Lee, S. Ando, and M. Kamionkowski, *The Gamma-Ray-Flux Probability Distribution Function from Galactic Halo Substructure*, *JCAP* **0907** (2009) 007, [[arXiv:0810.1284](#)].
  - [40] H.-S. Zechlin, A. Cuoco, F. Donato, N. Fornengo, and A. Vittino, *Unveiling the Gamma-ray Source Count Distribution Below the Fermi Detection Limit with Photon Statistics*, [arXiv:1512.07190](#).
  - [41] M. Lisanti, S. Mishra-Sharma, L. Necib, and B. R. Safdi, *Deciphering Contributions to the Extragalactic Gamma-Ray Background from 2 GeV to 2 TeV*, [arXiv:1606.04101](#).
  - [42] M. Ahlers and F. Halzen, *Pinpointing Extragalactic Neutrino Sources in Light of Recent IceCube Observations*, *Phys. Rev.* **D90** (2014), no. 4 043005, [[arXiv:1406.2160](#)].
  - [43] **Fermi-LAT** Collaboration, M. Ackermann et al., *GeV Observations of Star-forming Galaxies with Fermi LAT*, *Astrophys. J.* **755** (2012) 164, [[arXiv:1206.1346](#)].
  - [44] Q.-W. Tang, X.-Y. Wang, and P.-H. T. Tam, *Discovery of gev emission from the direction of the luminous infrared galaxy ngc 2146*, [arXiv:1407.3391](#).
  - [45] F.-K. Peng, X.-Y. Wang, R.-Y. Liu, Q.-W. Tang, and J.-F. Wang, *First detection of gev emission from an ultraluminous infrared galaxy: Arp 220 as seen with the fermi large area telescope*, [arXiv:1603.06355](#).
  - [46] **Fermi-LAT** Collaboration, F. Acero, M. Ackermann, et al., *Fermi large area telescope third source catalog*, [arXiv:1501.02003](#).
  - [47] C. Gruppioni et al., *The Herschel PEP/HerMES Luminosity Function. I: Probing the Evolution of PACS selected Galaxies to  $z$  4*, *Mon. Not. Roy. Astron. Soc.* **432** (2013) 23, [[arXiv:1302.5209](#)].
  - [48] **Fermi-LAT** Collaboration, M. Ackermann et al., *2FHL: The Second Catalog of Hard Fermi-LAT Sources*, *Astrophys. J. Suppl.* **222** (2016), no. 1 5, [[arXiv:1508.04449](#)].
  - [49] **Planck** Collaboration, P. Ade et al., *Planck 2013 results. XVI. Cosmological parameters*, *Astron. Astrophys.* **571** (2014) A16, [[arXiv:1303.5076](#)].
  - [50] **Fermi-LAT** Collaboration, M. Ackermann, M. Ajello, et al., *Resolving the extragalactic gamma-ray background above 50 gev with fermi-lat*, *arXiv* (2015) [[1511.00693](#)].
  - [51] M. Honda, M. Sajjad Athar, T. Kajita, K. Kasahara, and S. Midorikawa, *Atmospheric neutrino flux calculation using the NRLMSISE-00 atmospheric model*, *Phys. Rev.* **D92** (2015), no. 2 023004, [[arXiv:1502.03916](#)].
  - [52] R. Enberg, M. H. Reno, and I. Sarcevic, *Prompt neutrino fluxes from atmospheric charm*, *Phys. Rev.* **D78** (2008) 043005, [[arXiv:0806.0418](#)].
  - [53] F. Halzen and L. Wille, *Upper Limit on Forward Charm Contribution to Atmospheric Neutrino Flux*, [arXiv:1601.03044](#).
  - [54] R. Laha and S. J. Brodsky, *IC at IC: IceCube can constrain the intrinsic charm of the proton*, [arXiv:1607.08240](#).
  - [55] A. Bhattacharya, R. Enberg, Y. S. Jeong, C. S. Kim, M. H. Reno, I. Sarcevic, and A. Stasto, *Prompt atmospheric neutrino fluxes: perturbative qcd models and nuclear effects*, [arXiv:1607.00193](#).
  - [56] **IceCube** Collaboration, M. G. Aartsen et al., *Atmospheric and astrophysical neutrinos above 1 TeV interacting in IceCube*, *Phys. Rev.* **D91** (2015), no. 2 022001, [[arXiv:1410.1749](#)].
  - [57] **IceCube** Collaboration, M. G. Aartsen et al., *A combined maximum-likelihood analysis of the*

- high-energy astrophysical neutrino flux measured with IceCube*, *Astrophys. J.* **809** (2015), no. 1 98, [[arXiv:1507.03991](#)].
- [58] K. M. Gorski, E. Hivon, A. J. Banday, B. D. Wandelt, F. K. Hansen, M. Reinecke, and M. Bartelman, *Healpix – a framework for high resolution discretization, and fast analysis of data distributed on the sphere*, [astro-ph/0409513](#).
  - [59] M. Ahlers and F. Halzen, *Pinpointing Extragalactic Neutrino Sources in Light of Recent IceCube Observations*, *Phys. Rev.* **D90** (2014), no. 4 043005, [[arXiv:1406.2160](#)].
  - [60] P. A. Scheuer, *A statistical method for analysing observations of faint radio stars*, in *Mathematical Proceedings of the Cambridge Philosophical Society*, vol. 53, pp. 764–773, Cambridge Univ Press, 1957.
  - [61] X. Barcons, *Confusion noise and source clustering*, *The Astrophysical Journal* **396** (1992) 460–468.
  - [62] X. Barcons, G. Branduardi-Raymont, R. S. Warwick, A. C. Fabian, K. O. Mason, I. McHardy, and M. Rowan-Robinson, *Deep x-ray source counts from a fluctuation analysis of rosat pspc images*, *Monthly Notices of the Royal Astronomical Society* **268** (1994), no. 4 833–840, [<http://mnras.oxfordjournals.org/content/268/4/833.full.pdf+html>].
  - [63] **IceCube** Collaboration, M. G. Aartsen et al., *Energy Reconstruction Methods in the IceCube Neutrino Telescope*, *JINST* **9** (2014) P03009, [[arXiv:1311.4767](#)].
  - [64] **IceCube** Collaboration, T. Glüsenkamp, *Analysis of the cumulative neutrino flux from Fermi-LAT blazar populations using 3 years of IceCube data*, *EPJ Web Conf.* **121** (2016) 05006, [[arXiv:1502.03104](#)].
  - [65] S. Goodman, *Aligning statistical and scientific reasoning*, *Science* **352** (2016), no. 6290 1180–1181.
  - [66] J. D. Gibbons and J. W. Pratt, *P-values: Interpretation and methodology*, *The American Statistician* **29** (1975), no. 1 20–25, [<http://dx.doi.org/10.1080/00031305.1975.10479106>].
  - [67] A. C. Cohen, *Estimating the mean and variance of normal populations from singly truncated and doubly truncated samples*, *Ann. Math. Statist.* **21** (12, 1950) 557–569.
  - [68] M. Kadler et al., *Coincidence of a high-fluence blazar outburst with a PeV-energy neutrino event*, [arXiv:1602.02012](#).
  - [69] P. Padovani and E. Resconi, *Are both BL Lacs and pulsar wind nebulae the astrophysical counterparts of IceCube neutrino events?*, *Mon. Not. Roy. Astron. Soc.* **443** (2014), no. 1 474–484, [[arXiv:1406.0376](#)].
  - [70] M. Petropoulou, S. Dimitrakoudis, P. Padovani, A. Mastichiadis, and E. Resconi, *Photohadronic origin of gamma-ray BL Lac emission: implications for IceCube neutrinos*, *Mon. Not. Roy. Astron. Soc.* **448** (2015), no. 3 2412–2429, [[arXiv:1501.07115](#)].
  - [71] K. Emig, C. Lunardini, and R. Windhorst, *Do high energy astrophysical neutrinos trace star formation?*, *JCAP* **1512** (2015) 029, [[arXiv:1507.05711](#)].
  - [72] K. Fang, K. Kotera, M. C. Miller, K. Murase, and F. Oikonomou, *Identifying ultrahigh-energy cosmic-ray accelerators with future ultrahigh-energy neutrino detectors*, [arXiv:1609.08027](#).
  - [73] L. A. Anchordoqui, T. C. Paul, L. H. M. da Silva, D. F. Torres, and B. J. Vlcek, *What IceCube data tell us about neutrino emission from star-forming galaxies (so far)*, *Phys. Rev.* **D89** (2014), no. 12 127304, [[arXiv:1405.7648](#)].
  - [74] R. Moharana and S. Razzaque, *Angular correlation between icecube high-energy starting events and starburst sources*, [arXiv:1606.04420](#).
  - [75] **KM3NeT** Collaboration, S. Adrián-Martínez, M. Ageron, F. Aharonian, et al., *Letter of intent for km3net 2.0*, [arXiv:1601.07459](#).

- [76] **IceCube** Collaboration, D. F. Cowen, *Tau neutrinos in IceCube*, *J. Phys. Conf. Ser.* **60** (2007) 227–230.
- [77] **IceCube** Collaboration, M. G. Aartsen et al., *Search for Astrophysical Tau Neutrinos in Three Years of IceCube Data*, *Phys. Rev.* **D93** (2016), no. 2 022001, [[arXiv:1509.06212](#)].
- [78] G. J. Feldman and R. D. Cousins, *Unified approach to the classical statistical analysis of small signals*, *Physical Review D* **57** (1998), no. 7 3873–3889, [[physics/9711021](#)].
- [79] M. Yang, *Normal log-normal mixture, leptokurtosis and skewness*, *Applied Economics Letters* **15** (2008), no. 9 737–742, [<http://www.tandfonline.com/doi/pdf/10.1080/13504850600749073>].
- [80] V. V. Petrov, *Sums of independent random variables*, vol. 82. Springer, 1975.
- [81] M. Tai, *A mathematical model for the determination of total area under glucose tolerance and other metabolic curves*, *Diabetes Care* **17** (1994), no. 2 152–154.
- [82] A. Palladino, G. Pagliaroli, F. L. Villante, and F. Vissani, *What is the Flavor of the Cosmic Neutrinos Seen by IceCube?*, *Phys. Rev. Lett.* **114** (2015), no. 17 171101, [[arXiv:1502.02923](#)].
- [83] J. Glenn, A. Conley, M. Béthermin, et al., *Hermes: deep galaxy number counts from a  $p(d)$  fluctuation analysis of spire science demonstration phase observations*, *Monthly Notices of the Royal Astronomical Society* **409** (2010), no. 1 109–121, [<http://mnras.oxfordjournals.org/content/409/1/109.full.pdf+html>].
- [84] H.-S. Zechlin, A. Cuoco, F. Donato, N. Fornengo, and M. Regis, *Statistical Measurement of the Gamma-ray Source-count Distribution as a Function of Energy*, [arXiv:1605.04256](#).
- [85] J. J. Condon, W. D. Cotton, E. B. Fomalont, K. I. Kellermann, N. Miller, R. A. Perley, D. Scott, T. Vernstrom, and J. V. Wall, *Resolving the Radio Source Background: Deeper Understanding Through Confusion*, *Astrophys. J.* **758** (2012) 23, [[arXiv:1207.2439](#)].
- [86] T. Vernstrom, D. Scott, J. V. Wall, J. J. Condon, W. D. Cotton, E. B. Fomalont, K. I. Kellermann, N. Miller, and R. A. Perley, *Deep 3 GHz number counts from a  $P(D)$  fluctuation analysis*, *Mon. Not. Roy. Astron. Soc.* **440** (2014), no. 3 2791–2809, [[arXiv:1311.7451](#)].
- [87] P. C. Breyse, E. D. Kovetz, and M. Kamionkowski, *Carbon monoxide intensity mapping at moderate redshifts*, *Monthly Notices of the Royal Astronomical Society* **443** (2014), no. 4 3506–3512, [<http://mnras.oxfordjournals.org/content/443/4/3506.full.pdf+html>].
- [88] P. C. Breyse, E. D. Kovetz, and M. Kamionkowski, *The high-redshift star formation history from carbon-monoxide intensity maps*, *Monthly Notices of the Royal Astronomical Society: Letters* **457** (2016), no. 1 L127–L131, [<http://mnrasl.oxfordjournals.org/content/457/1/L127.full.pdf+html>].
- [89] P. C. Breyse, E. D. Kovetz, P. S. Behroozi, L. Dai, and M. Kamionkowski, *Insights from probability distribution functions of intensity maps*, [arXiv:1609.01728](#).
- [90] **Pierre Auger** Collaboration, P. Abreu et al., *Ultrahigh Energy Neutrinos at the Pierre Auger Observatory*, *Adv. High Energy Phys.* **2013** (2013) 708680, [[arXiv:1304.1630](#)].
- [91] P. W. Gorham et al., *Observational constraints on the ultrahigh energy cosmic neutrino flux from the second flight of the anita experiment*, *Physical Review D* **82** (2010), no. 2 [[1003.2961](#)].
- [92] P. W. Gorham et al., *Erratum: Observational constraints on the ultrahigh energy cosmic neutrino flux from the second flight of the anita experiment [phys. rev. d, 82, 022004 (2010)]*, *Physical Review D* **85** (2012), no. 4 [[1011.5004](#)].